Going from microscopic to macroscopic on nonuniform growing domains

Christian A. Yates,[1,*] Ruth E. Baker,[1,†] Radek Erban,[2,‡] and Philip K. Maini[1,§]

[1]*Centre for Mathematical Biology, Mathematical Institute, University of Oxford, 24-29 St Giles', Oxford OX1 3LB, United Kingdom*

[2]*Centre for Mathematical Biology and Oxford Centre for Collaborative Applied Mathematics, Mathematical Institute, University of Oxford, 24-29 St Giles', Oxford OX1 3LB, United Kingdom*

(Received 16 April 2012; revised manuscript received 28 June 2012; published 23 August 2012)

Throughout development, chemical cues are employed to guide the functional specification of underlying tissues while the spatiotemporal distributions of such chemicals can be influenced by the growth of the tissue itself. These chemicals, termed morphogens, are often modeled using partial differential equations (PDEs). The connection between discrete stochastic and deterministic continuum models of particle migration on growing domains was elucidated by Baker, Yates, and Erban [Bull. Math. Biol. **72**, 719 (2010)] in which the migration of individual particles was modeled as an on-lattice position-jump process. We build on this work by incorporating a more physically reasonable description of domain growth. Instead of allowing underlying lattice elements to instantaneously double in size and divide, we allow incremental element growth and splitting upon reaching a predefined threshold size. Such a description of domain growth necessitates a nonuniform partition of the domain. We first demonstrate that an individual-based stochastic model for particle diffusion on such a nonuniform domain partition is equivalent to a PDE model of the same phenomenon on a nongrowing domain, providing the transition rates (which we derive) are chosen correctly and we partition the domain in the correct manner. We extend this analysis to the case where the domain is allowed to change in size, altering the transition rates as necessary. Through application of the master equation formalism we derive a PDE for particle density on this growing domain and corroborate our findings with numerical simulations.

DOI: 10.1103/PhysRevE.86.021921 PACS number(s): 87.10.Mn, 87.17.Aa, 87.17.Ee, 87.17.Jj

I. INTRODUCTION

When modeling particle diffusion we have a choice between macroscopic population-based models and micro- or mesoscopic individual-based models. The latter are often formulated as a population of individuals undergoing an on-lattice random walk [1–3]. Considering multiple short bursts of experimental data, it may be possible to derive the coefficients of a microscopic Fokker-Planck equation (FPE) or, equivalently, a stochastic differential equation, which describes the movement rules for individual particles, using the so-called equation-free technique [4,5]. This approach has been successful for the modeling of biological motion on larger scales, specifically for locust movement [6,7]. It may also be possible to derive the transition rates for a mesoscopic position-jump model by simply overlaying a grid on experimental data.

However, these micro- or mesoscopic models are generally mathematically intractable and, when considering large numbers of individuals, will take (in general) orders of magnitude longer to simulate than macroscopic population-based models. Additionally, macroscopic models are often more straightforward to write down and are easier and faster to simulate, especially for large particle numbers. Partial differential equation (PDE) models are also amenable to mathematical analysis via a range of well characterized techniques.

We first present a macroscopic approach in which a characteristic of the whole population is considered directly. This approach leads to a PDE model where the diffusion of particles can be modeled by analogy to Fick's law

$$\frac{\partial u}{\partial t} = \nabla \cdot (D \nabla u). \tag{1}$$

The derivation of a macroscopic diffusion coefficient D from a microscopic model is relatively simple for many microscopic models [8], although it can be decidedly more difficult when particles are modeled as having a finite size rather than being point particles, as in the case of the cellular Potts model [9,10]. For some models the diffusion coefficient D depends on the particle density u [2,11]. In some cases it may even be replaced by a more general (anisotropic) diffusion tensor, obtained by the diffusion approximation of the transport equation that describes the underlying random walk model [12,13].

A. Incorporating domain growth

Using standard conservation of matter arguments, as in the case of the stationary domain, in combination with Reynolds transport theorem, we can alter the classical diffusion equation (1) to account for a time-dependent growing domain $\Omega(t)$. We arrive at the following PDE for the particle density $u(\boldsymbol{x},t)$:

$$\frac{\partial u}{\partial t} + \nabla \cdot (\boldsymbol{v} u) = \nabla \cdot (D \nabla u), \quad (\boldsymbol{x},t) \in \Omega(t) \times [0,\infty), \tag{2}$$

where $\boldsymbol{v}(\boldsymbol{x},t) = d\boldsymbol{x}/dt$ is the velocity field generated by domain growth (see Ref. [14] for a detailed derivation).

In a previous work [14] we demonstrated an equivalence between a stochastic individual-based model (a position-jump model on a regular underlying lattice of elements)

*yatesc@maths.ox.ac.uk; http://people.maths.ox.ac.uk/yatesc/
†baker@maths.ox.ac.uk; http://people.maths.ox.ac.uk/baker/
‡erban@maths.ox.ac.uk; http://people.maths.ox.ac.uk/erban/
§maini@maths.ox.ac.uk; http://people.maths.ox.ac.uk/maini/

 ©2012 American Physical Society

incorporating domain growth and a continuum representation of the form of equation (2). Domain growth was implemented through the instantaneous doubling and dividing of underlying lattice elements. We would like to move away from this unphysical description of growth to a model where the underlying lattice elements grow and divide in a more natural, continuous way. Stochasticity will be introduced by making growth of the individual tissue elements a random process. The consideration of domain elements of differing sizes motivates the consideration of nonuniform domains. We expect that this work will provide us with a more realistic method of simulating stochastic pattern formation on growing domains. Potential biological application areas include modeling the movement of cells in response to chemical signals [1] and the simulation of morphogen concentrations on developing embryos [15] among others [16].

B. Outline

As an introduction to the area we will briefly summarize our previous work on the equivalence between stochastic and continuum models of diffusion in one dimension both with and without domain growth [14]. In Ref. [14] we were able to incorporate the important two-way feedback between particle density and domain growth into the equivalence framework. In this paper, however, we will focus purely on the technical aspects of incorporating nonuniform domain partitions into our equivalence framework and leave inclusion of the dependence of domain growth on particle density for future work. In Sec. III the desire for a more physically reasonable description of domain growth will stimulate us to consider stochastic models with nonuniform domain division, which we will investigate initially on a nongrowing one-dimensional domain. We also discuss the important distinction between two different types of domain partition, which were equivalent on the uniform domain. In Sec. IV domain growth will be introduced. In Sec. V we demonstrate an equivalence between our model and a PDE describing the change in particle density across the growing domain by consideration of a master equation. We corroborate our findings in Sec. VI with numerical simulations that demonstrate the equivalence of the two models. In Sec. VII we conclude with a short discussion of the limitations and possible consequences of our work.

II. MODELING PARTICLE MIGRATION IN FIXED DOMAINS

All the individual, particle-based stochastic models outlined in this paper consider some fixed (unless otherwise stated) population of $\mathcal{N}$ particles restricted to move on a finite domain. The domain is not, for the moment, considered to be biological tissue. Instead we consider a general framework that will allow us to subsequently incorporate biologically motivated features. Nevertheless, we still refer to an individual section of the domain as a tissue element, interval, or box throughout the rest of this paper. Particles are allowed to move via random diffusion. We assume, unless explicitly stated, that there are no reactions between particles and no particle degradation on the time scale of interest and that particles may not enter or leave the domain, although such effects could be easily incorporated into our framework and have been in other similar frameworks (see Ref. [14]). These zero flux boundary conditions in combination with the absence of particle creation or degradation render the population constant in time. The first model presented for this process is at a discrete particle level in which all the particles are modeled as identical individuals moving subject to probabilistic rules.

Consider the nondimensionalized stationary (time-independent) domain $x \in [0,1]$ discretized into k intervals each of length $\Delta x = 1/k$. Here Δx will be known as the standard interval length. The random variable denoting the number of particles in interval i is N_i and the evolution of particle numbers over the whole domain can be denoted by the vector $\boldsymbol{N}(t) = [N_1(t), N_2(t), \ldots, N_k(t)]$ (On the uniform grid, described here, particle density and particle numbers will scale by a constant factor - the length of a tissue interval - so that we can use the terms almost interchangeably. However, when we come to consider a nonuniform domain partition the numbers of particles in each interval must be divided by the length of that interval in order to calculate the particle density in that part of the domain). Initially, in this stochastic position-jump model, we assume that the particles are restricted to move on a spatial grid between points defined to be at the center of each element and we denote the transition rates for a particle to move out of interval i to the left as T_i^- and to the right as T_i^+. These rates may depend on the particle density $\boldsymbol{N}$, external signaling factors $\boldsymbol{s}$, and time t. To complete the formulation of the model we specify initial and boundary conditions. In order to model the conservation of particles on the domain we assume $T_1^- = T_k^+ = 0$. This is analogous to zero flux boundary conditions in a continuum model. Each interval is initialized to contain a particular number of particles so that the total number across the domain sums to $\mathcal{N}$.

It is possible to construct a reaction-diffusion master equation (RDME) describing the evolution of particle density $\boldsymbol{N}$. Let $\text{Prob}(\boldsymbol{n},\boldsymbol{s},t)$ be the joint probability that $\boldsymbol{N} = \boldsymbol{n}$ at time t under deterministic external conditions $\boldsymbol{s}$ with $\boldsymbol{n} = [n_1, n_2, \ldots, n_k]$ and $\boldsymbol{s} = [s_1, s_2, \ldots, s_k]$ and define the operators $J_i^+ : \mathbb{R}^k \to \mathbb{R}^k$ for $i = 1, \ldots, k-1$ and $J_i^- : \mathbb{R}^k \to \mathbb{R}^k$ for $i = 2, \ldots, k$ by

$$\begin{aligned} J_i^+ &: [n_1, \ldots, n_i, \ldots, n_k] \\ &\quad \to [n_1, \ldots, n_{i-2}, n_{i-1}, n_i + 1, n_{i+1} - 1, n_{i+2} \ldots, n_k], \\ J_i^- &: [n_1, \ldots, n_i, \ldots, n_k] \\ &\quad \to [n_1, \ldots, n_{i-2}, n_{i-1} - 1, n_i + 1, n_{i+1}, n_{i+2} \ldots, n_k]. \end{aligned}$$

By considering all the possible particle movements in a time interval δt, small enough that the probability of more than one particle movement in δt is $O(\delta t)$, we can write the RDME as follows [14]:

$$\begin{aligned} \frac{\partial\, \text{Prob}(\boldsymbol{n},t)}{\partial t} &= \sum_{i=1}^{k-1} T_i^+ \{(n_i + 1)\text{Prob}(J_i^+ \boldsymbol{n}, \boldsymbol{s}, t) - n_i \text{Prob}(\boldsymbol{n}, \boldsymbol{s}, t)\} \\ &\quad + \sum_{i=2}^{k} T_i^- \{(n_i + 1)\text{Prob}(J_i^- \boldsymbol{n}, \boldsymbol{s}, t) - n_i \text{Prob}(\boldsymbol{n}, \boldsymbol{s}, t)\}. \quad (3) \end{aligned}$$

Consider the vector of stochastic means, defined as

$$\boldsymbol{M}(t) = [M_1(t), \ldots, M_k(t)] = \sum_{\boldsymbol{n}} \boldsymbol{n}\,\mathrm{Prob}(\boldsymbol{n},\boldsymbol{s},t)$$

$$\equiv \sum_{n_1=0}^{\infty}\sum_{n_2=0}^{\infty}\cdots\sum_{n_k=0}^{\infty} \boldsymbol{n}\,\mathrm{Prob}(\boldsymbol{n},\boldsymbol{s},t). \tag{4}$$

It can be demonstrated that these means satisfy

$$\frac{dM_1}{dt} = T_2^- M_2 - T_1^+ M_1, \tag{5}$$

$$\frac{dM_i}{dt} = T_{i-1}^+ M_{i-1} - (T_i^+ + T_i^-)M_i + T_{i+1}^- M_{i+1} \quad \text{for} \quad i = 2, \ldots, k-1, \tag{6}$$

$$\frac{dM_k}{dt} = T_{k-1}^+ M_{k-1} - T_k^- M_k, \tag{7}$$

providing $T_i^{\pm}$ is independent of particle density [1,14]. Equation (6) is similar to the master equation for the positional probability of a random walker on a lattice as derived by Othmer and Stevens [1] and Painter and Hillen [2].

To draw a rigorous correspondence between Eqs. (5)–(7) and a population-level description of the variation of particle density with time, terms of the form $M_{i\pm1} = M(x_i \pm \Delta x, t)$ are expanded about x_i. Taking transition rates $T_i^{\pm} = d$ for $i = 1, \ldots, k$, for example, gives

$$\frac{\partial M}{\partial t}(x_i,t) = d(\Delta x)^2 \frac{\partial^2 M}{\partial x^2}(x_i,t) + O((\Delta x)^2), \tag{8}$$

where $M(x_i,t) = M_i$. Here $\Delta x = 1/k$, the distance between the centers of the intervals, is the same as the length of each interval. Allowing $\Delta x \to 0$ in such a way [1] that $\lim_{\Delta x\to 0} d(\Delta x)^2 = D$ gives the diffusion equation for particle density, $u(x,t)$:

$$\frac{\partial u}{\partial t} = D\frac{\partial^2 u}{\partial x^2}, \quad (x,t) \in [0,1] \times [0,\infty). \tag{9}$$

Conservation of particles in the deterministic model can be derived from the moment equations and correspond to zero flux boundary conditions on u:

$$\left.\frac{\partial u}{\partial x}\right|_{x=0,1} = 0. \tag{10}$$

III. PARTICLE DIFFUSION ON A NONUNIFORM DOMAIN

In order to consider a more physically reasonable approach to domain growth than in previous studies (see Ref. [14]), we would like to allow the underlying domain elements to grow by small increments and then divide upon reaching a critical size rather than instantaneously doubling in size and dividing as has previously been implemented (see Fig. 1). Incorporating incremental stochastic interval growth necessitates the consideration of domain elements of different sizes. This will affect transition rates between the elements. For example, if, in a microscopic model, a particle is assumed to be exhibiting an unbiased, Brownian random walk it will take longer, on average, for that particle to exit a larger element than a smaller one. To begin with we will characterize the diffusion process on a nongrowing, nonuniform domain, deriving transition rates for tissue elements of different sizes. Once the correct transition rates have been established on the stationary domain we will attempt to incorporate growth into the one-dimensional model.

A. Particle migration on a stationary, nonuniform grid

Now that we are considering a nonuniform grid we must be careful about how we define our domain partition. There are two natural ways to do this (see Fig. 2).

(i) Points $x_1, x_2, \ldots, x_k$ are chosen and are associated with intervals $1, \ldots, k$, respectively. The interval edges $y_0 = 0$, $y_k = 1$, and $y_i = (x_i + x_{i+1})/2$, for $i = 1, \ldots, k-1$, are then

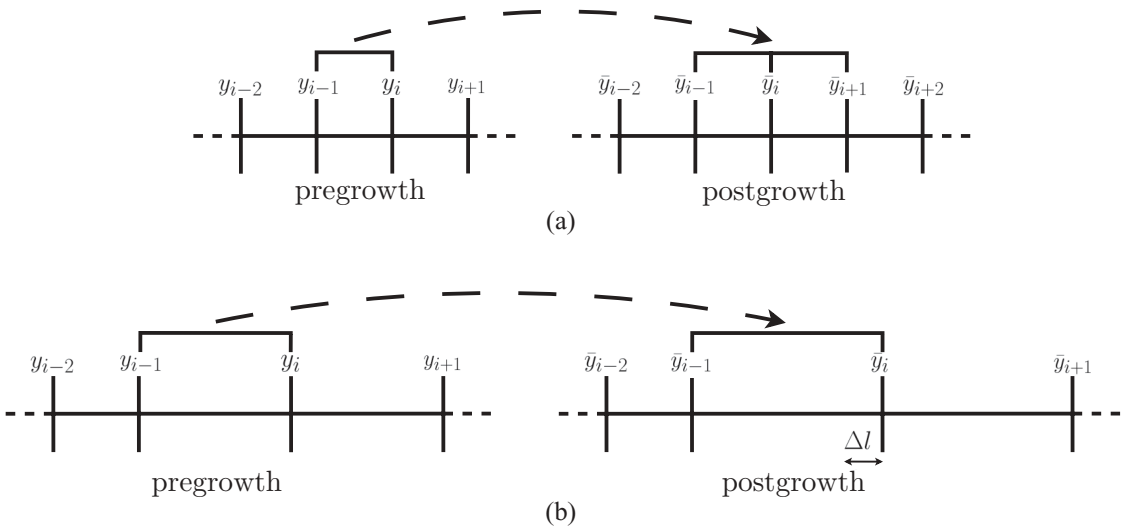

FIG. 1. Two different implementations of discrete domain growth. (a) Originally the interval instantaneously doubles and splits. Interval i is selected to grow. This interval doubles in size and splits down the middle creating two daughter intervals of the same size as the original. All intervals with index greater than i are shifted to the right by one interval length Δx and their indices are increased by one. All intervals remain the same size as each other. (b) The incremental growth method defined herein. Interval i is selected to grow. The interval is made larger by a small amount Δl and all intervals with index greater than i are shifted to the right by Δl. Interval division does not take place until an interval grows to a prespecified size. This method introduces inhomogeneity in interval size.

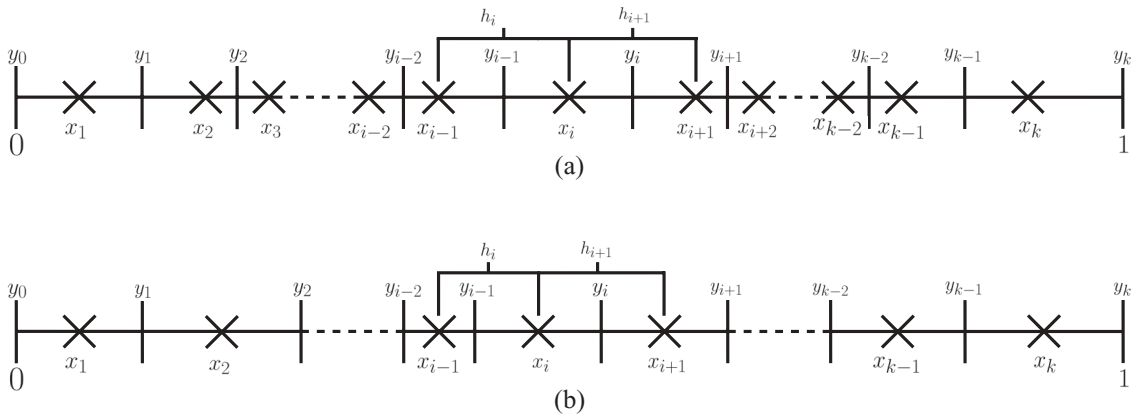

FIG. 2. Two different domain partitions. (a) The Voronoi partition method. Particle positions x_i are chosen first and interval i is defined to be all the points that lie closer to x_i than any of the other particle positions x_j for $j \neq i$. This gives interval edges at $y_i = (x_i + x_{i+1})/2$. The Voronoi partition method allows for the natural incorporation of transition rates that are inversely proportional to interval size, which cannot be done within the interval-centered framework. (b) The interval-centered definition. Interval boundaries y_i are defined first and particles are assumed to lie in the centers of these intervals. In both partitions the distance between neighboring particle positions x_i and x_{i-1} is denoted $h_i = x_i - x_{i-1}$ and similarly $h_{i+1} = x_{i+1} - x_i$. For the end intervals indexed 1 and k, h_1 and h_{k+1} are not defined, so we choose $h_1 = 2x_1$ and $h_{k+1} = 2(y_k - x_k)$ for consistency with later results.

naturally defined in a Voronoi neighborhood sense: A point on the domain is defined to lie in the interval i if it is nearer to x_i than any other x_j for $j = 1, \ldots, k$, $j \neq i$.

(ii) The edges of the intervals $y_0, y_1, \ldots, y_k$ are chosen (with $y_0 = 1$ and $y_k = 1$ defining the end points of the domain) and the point x_i associated with interval i, for $i = 1, \ldots, k$, is defined to be the center of that interval [i.e., $x_i = (y_{i-1} + y_i)/2$ for $i = 1, \ldots, k$].

The Voronoi domain partition is the natural particle-position-focused extension of the uniform domain partition. The positions where the particles are considered to lie are defined first and the interval boundaries are defined to bisect these points. The interval-centered domain partition is the natural interval-focused extension of the uniform domain partition. The intervals are defined first and the positions where the particles lie are placed at the center of the intervals. On the uniform grid, these two interval definitions are equivalent, but there is an important distinction to be made on the nonuniform grid: using definition (ii), the centers of each interval will no longer correspond to the Voronoi points. The second method of defining intervals gives increased control over the sizes and shapes of the individual intervals, but we will show that it leads to incorrect particle densities when implementing stochastic simulations (see Fig. 4 and Sec. S.1 of Ref. [17]). It is therefore important to implement the Voronoi property in order to choose transition rates that lead both to the correct particle densities in each interval for stochastic simulations and to the correct corresponding macroscopic PDE. [That is, given a set of points, $x_1, x_2, \ldots, x_k$, associated with each interval, the number of particles at x_i is independent of how we define the boundaries of the intervals, since (as we will demonstrate) transition rates are only dependent on the distances between neighboring points. However, when we come to calculating particle densities the interval boundaries become important and we can show (see Sec. S.1 of Ref. [17]) that the Voronoi domain partition gives smoothly varying particle densities, which correspond to the derived PDE, because the interval sizes are related to the transition rates in a unique way.] In what follows we primarily use the first method to partition our domain into intervals (known hereafter as Voronoi partitioning). We will, however, give comparisons of the two partition methods on both fixed and growing domains demonstrating the propriety of the Voronoi partition. In Sec. IV C we also discuss when it might be more appropriate to use the interval-centered domain partition to increase our control over the interval sizes.

The Voronoi partition implies that the boundaries for interval i will be at $y_{i-1} = (x_{i-1} + x_i)/2$ (left-hand boundary) and $y_i = (x_i + x_{i+1})/2$ (right-hand boundary). As in the case of the uniform domain, particles are considered to be positioned at $x_1, x_2, \ldots, x_k$ for intervals $1, \ldots, k$, respectively (see Fig. 2). Intervals $2, \ldots, k-1$ will be known as interior intervals and intervals 1 and k as end intervals.

Previously, the scalings of the transition rates for particles to move between intervals have been specified somewhat artificially by considering Eqs. (5)–(7) (or their analogs), Taylor expanding the terms at $i \pm 1$, and choosing the scaling so that we return to a macroscopic PDE [1]. Now that we are considering a nonuniform domain it is not so simple to see what the requisite scaling for each transition rate should be. In order to ensure correspondence with a PDE the transition rates should depend in some way on the sizes of the intervals between which a particle moves. Even if we could guess the transition rates and plug them into Eqs. (5)–(7) to check that we derive the correct macroscale equation, it would be preferable to have a microscale justification of these scalings. The transition rate for a particle at x_i should depend on the distance to the associated domain definition points in the neighboring intervals x_{i-1} and x_{i+1}. As such, we consider a microscale migration process in the interval $[x_{i-1}, x_{i+1}]$. We will consider this microscale process to be simple Brownian motion and expect to derive transition rates that lead us, via our mesoscale position-jump process, to the diffusion equation on the macroscale. It is also possible to consider

alternative underlying microscale processes that correspond to biased and/or correlated random walks and give rise to advection-diffusion PDEs.

B. From microscopic to mesoscopic

A particle moving according to Brownian motion, with position $X(t)$, obeys a stochastic differential equation (SDE)

$$dX(t) = \sqrt{2D}dW_t, \tag{11}$$

where dW_t is a standard Wiener process and D is the diffusion coefficient of the diffusion equation corresponding to this SDE. The probability density function of the particle $p(x,t)$ evolves according to the classical diffusion equation

$$\frac{\partial p(x,t)}{\partial t} = D\frac{\partial^2 p(x,t)}{\partial x^2}. \tag{12}$$

Given that we know the initial position of the particle x_i, we have a δ function initial condition, $p(x,t) = \delta(x - x_i)$. Finding the transition rates for the mesoscale position-jump process reduces to a first passage problem. In order to find the transition rate for moving out of interval i in the position-jump model, we consider the process in which a particle starting at x_i exits the interval $[x_{i-1},x_{i+1}]$ and find the probability for it to do so at either end. The interval $[x_{i-1},x_{i+1}]$ is the appropriate interval for the calculation of the first passage time since it requires that the particle finishes its transition in an equivalent position, in an adjacent interval, to the position at which it started in the original interval. The absorbing boundary conditions $p(x_{i-1},t) = p(x_{i+1},t) = 0$ complete the formulation of the above problem. This is a classic first passage problem, the likes of which are dealt with thoroughly by Redner [18]. Note that the formulation of the first passage problem and hence the transition rates between intervals is independent of the position of the interval boundaries. Here we briefly summarize Redner's derivation of the mean first passage time.

We first calculate the probabilities for the particle to leave at either end of the interval, known as the eventual hitting probabilities,

$$\varepsilon_-(x_i) = \frac{x_{i+1} - x_i}{x_{i+1} - x_{i-1}}, \tag{13}$$

$$\varepsilon_+(x_i) = \frac{x_i - x_{i-1}}{x_{i+1} - x_{i-1}}. \tag{14}$$

We next calculate the conditional mean exit times to leave the interval at either end,

$$\langle t(x_i)\rangle_- = \frac{(x_i - x_{i-1})(2x_{i+1} - x_i - x_{i-1})}{6D}, \tag{15}$$

$$\langle t(x_i)\rangle_+ = \frac{(x_{i+1} - x_i)(x_{i+1} + x_i - 2x_{i-1})}{6D}, \tag{16}$$

which we can use in conjunction with the eventual hitting probabilities [see Eqs. (13) and (14)] to calculate the unconditional mean exit time from the interval,

$$\begin{aligned}\langle t(x_i)\rangle &= \varepsilon_-(x_i)\langle t(x_i)\rangle_- + \varepsilon_+(x_i)\langle t(x_i)\rangle_+ \\ &= \frac{1}{2D}(x_i - x_{i-1})(x_{i+1} - x_i).\end{aligned} \tag{17}$$

We can invert this to give the unconditional mean exit rate and by multiplying through by the eventual hitting probabilities calculate the conditional mean exit rates or transition rates,

$$T_i^- = \frac{2D}{h_i(h_i + h_{i+1})}, \tag{18}$$

$$T_i^+ = \frac{2D}{h_{i+1}(h_i + h_{i+1})}, \tag{19}$$

where, for brevity, as previously defined, we denote $h_i = x_i - x_{i-1}$ and similarly $h_{i+1} = x_{i+1} - x_i$. These transition rates are the same as those derived by Engblom *et al.* [19] using a finite element discretization of the macroscopic diffusion equation.

Recall the equations relating the mean numbers of particle in each interval (5)–(7):

$$\begin{aligned}\frac{dM_1}{dt} &= T_2^- M_2 - T_1^+ M_1, \\ \frac{dM_i}{dt} &= T_{i-1}^+ M_{i-1} - (T_i^+ + T_i^-)M_i + T_{i+1}^- M_{i+1}, \\ &\qquad i = 2,\ldots,k-1, \\ \frac{dM_k}{dt} &= T_{k-1}^+ M_{k-1} - T_k^- M_k.\end{aligned}$$

Although these equations were derived initially for a uniform mesh, they remain valid for the nonuniform mesh. We can rewrite this equation in terms of particle densities $u_i = M_i/l_i$, where l_i is the length of interval i:

$$\frac{du_1}{dt} = \frac{1}{l_1}(T_2^- u_2 l_2 - T_1^+ u_1 l_1), \tag{20}$$

$$\frac{du_i}{dt} = \frac{1}{l_i}[T_{i-1}^+ u_{i-1} l_{i-1} - (T_i^+ + T_i^-)u_i l_i + T_{i+1}^- u_{i+1} l_{i+1}], \quad i = 2,\ldots,k-1, \tag{21}$$

$$\frac{du_k}{dt} = \frac{1}{l_k}(T_{k-1}^+ u_{k-1} l_{k-1} - T_k^- u_k l_k). \tag{22}$$

We now use Taylor series expansions about position x_i on the appropriate terms. For example,

$$\begin{aligned}u_{i+1} &= u(x_{i+1}) \\ &= u(x_i) + (h_{i+1})\frac{\partial u}{\partial x}(x_i) + \frac{1}{2}(h_{i+1})^2\frac{\partial^2 u}{\partial x^2}(x_i) + \cdots.\end{aligned} \tag{23}$$

Allowing the number of domain elements k to tend to infinity on the Voronoi domain partition (i.e., with the appropriate choices of l_i), implying $h_i, h_{i+1} \to 0\ \forall\ i$, we obtain the diffusion equation for particle density $u(x,t)$:

$$\frac{\partial u}{\partial t} = D\frac{\partial^2 u}{\partial x^2} \quad \text{for} \quad (x,t) \in [0,1]\times[0,\infty), \tag{24}$$

with the usual zero flux boundary conditions. For a more detailed derivation and a justification of the necessity of the Voronoi domain partition see Sec. S.1 of Ref. [17].

Figure 3 shows a numerical comparison of the stochastic simulations and the derived PDE (24). Qualitatively, the PDE for particle density matches the particle density of the stochastic simulations well. In Fig. 3(f), in order to give a more quantitative comparison of the two simulation types, we have plotted the variation of the histogram distance error or metric between the stochastic particle density and the PDE,

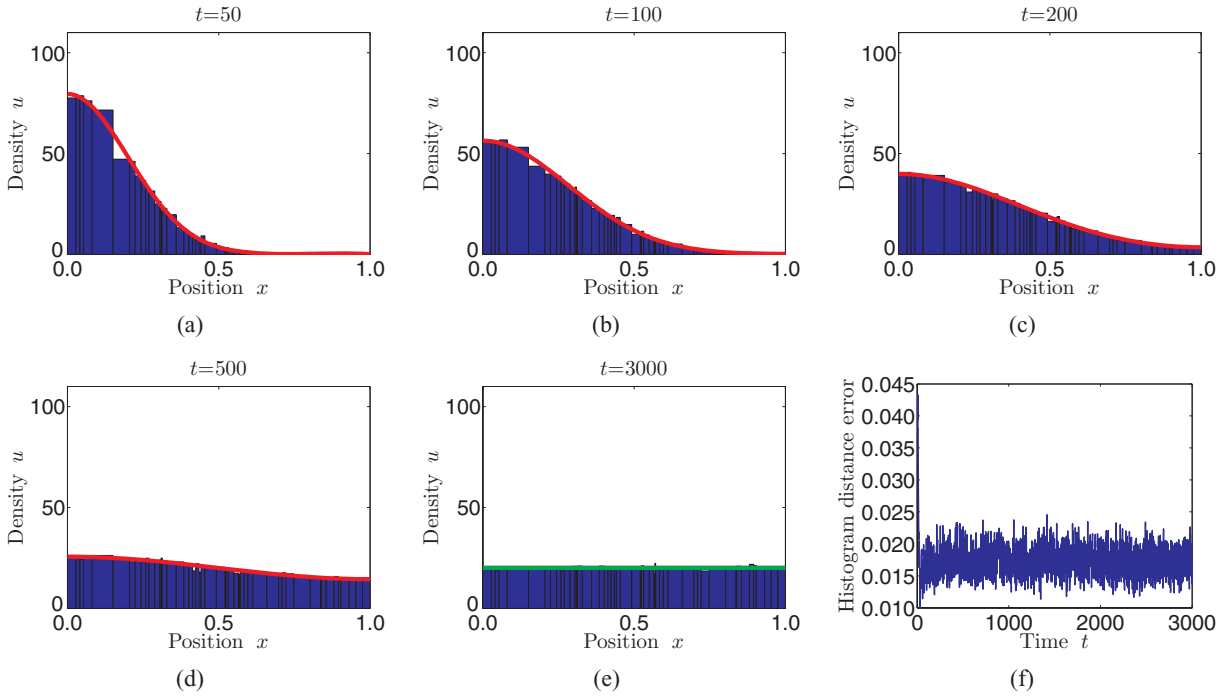

FIG. 3. (Color online) Particles diffusing with constant rate at several time points. (a)–(e) Histograms represent an average of 40 stochastic realizations of the system with transition rates given by Eqs. (18) and (19). The red (dark gray) curves represent the solution of the PDE (24) and the green (light gray) curve in (e) represents the steady state solution of the PDE found analytically. The green (light gray) curve is plotted in order to demonstrate the agreement of the stochastic simulation algorithm, the numerical solution of the PDE, and the analytical solution at steady state. The agreement is good, with the analytically derived green (light gray) curve lying exactly on top of, and so obscuring, the numerically computed curve. (f) Evolution of the histogram distance error between the stochastic simulations and the PDE. All $\mathcal{N} = 1000$ particles are released from the Voronoi point associated with the first interval. The macroscopic diffusion coefficient takes the value $D = \Delta x^2$, where $\Delta x = 1/k$ and $k = 50$. For a video of the evolution of particle density please see movie Fig. 3.avi of Ref. [17]. (For interpretation of the references to color in this and other figures in this paper, the reader is referred to the online version of this article.)

over time. The histogram distance metric between two curves (defined at discrete points), having normalized frequencies a_i and b_i at point i (i.e., $\sum a_i = \sum b_i = 1$), is given by

$$D = \frac{\sum |a_i - b_i|}{2}, \tag{25}$$

where the sum is over all i such that either $a_i \neq 0$ or $b_i \neq 0$. Since our particle densities are defined at nonregular lattice points x_i, we interpolate the value of the PDE at each lattice point in order to compare the curves. Figure 3(f) shows a low histogram distance error for the duration of the simulation, indicating good agreement between the two simulation types.

For all simulations we employ Gillespie's exact direct method stochastic simulation algorithm [20] and release all $\mathcal{N} = 1000$ particle from x_1, the Voronoi point of the first interval.

C. Using a mixed boundary interval to derive transition rates for the end intervals

In order to implement zero flux boundary conditions on the macroscopic domain we designate the left-hand end of the first interval and the right-hand end of the last interval at zero and one, respectively, to be reflecting boundaries. We can carry out an analysis similar to that above in order to find the correct mesoscopic jump rates from an underlying microscopic process. Without loss of generality we will assume that we are considering the right-hand end interval $[y_{k-1}, y_k]$ of the position-jump process. In order to derive the transition rates we consider the behavior of a particle initially at x_k on the domain $[x_{k-1}, y_k]$ where we impose an absorbing boundary condition at $x = x_{k-1}$ and a reflecting boundary condition at $x = y_k = 1$.

Employing a similar method as was used for an underlying microscopic diffusion process in the case of two absorbing boundaries [18], we can calculate the conditional hitting probabilities at $x = x_{k-1}$ and 1 to be

$$\varepsilon_-(x_k) = 1, \quad \varepsilon_+(x_k) = 0, \tag{26}$$

which implies we are certain to exit the interval at the left-hand boundary, which is to be expected. We can calculate the conditional mean exit time at the left-hand boundary as

$$\langle t(x_k) \rangle_- = \frac{1}{2D}\left[2(y_k - x_{k-1})h_k - h_k^2\right]. \tag{27}$$

Rearranging gives the transition rate as

$$T_k^- = \frac{2D}{h_k[2(y_k - x_{k-1}) - x_k + x_{k-1}]} = \frac{2D}{h_k(h_k + h_{k+1})}, \tag{28}$$

recalling the definitions $h_1 = 2x_1$ and $h_k = 2(y_k - x_k)$. In an entirely analogous manner we can derive the transition rate to

move right out of the first interval as

$$T_1^+ = \frac{2D}{h_2(x_2 + x_1)} = \frac{2D}{h_2\,(h_1 + h_2)}. \tag{29}$$

On the uniform domain these transition rates reduce to

$$T_k^- = T_1^+ = \frac{D}{h^2}, \tag{30}$$

as we might reasonably expect.

D. Comparison with the interval-centered domain partition

In order to demonstrate the propriety of the Voronoi domain partition in comparison to the interval-centered domain partition we have carried out simulations similar to those detailed above with the interval-centered domain partition. The transition rates are the same as those derived in preceding sections [see Eqs. (18) and (19) in Sec. III B and Eqs. (28) and (29) in Sec. III C] only now the positions x_i where particles are assumed to reside are the centers of the corresponding intervals. It is evident from glancing at Figs. 4(a)–4(e) that the particle densities deviate significantly from the mean-field description for the vast majority of the intervals. This is reinforced quantitatively by considering Fig. 4(f). For the majority of the simulation the histogram distance error takes values that are more than an order of magnitude larger than those in the analogous Voronoi partition simulations.

Initializing each repeat of the stochastic simulation with the same interval-centered partition gives aberrant particle densities. However, if the domain partition is different for each repeat of the simulation then the errors can balance themselves out, leading to an improved comparison to the particle density given by the PDE. We give further details of this phenomenon for the stationary domain in Sec. S.2 of Ref. [17] and for the growing domain in Sec. VI of this paper.

IV. PARTICLE MIGRATION WITH DOMAIN GROWTH

Previously, growth has been implemented using interval splitting, where an interval doubles in length and divides instantaneously [14]. In order to represent the growth of the underlying tissue intervals more realistically it is preferable to allow intervals to grow by small increments (more akin to a continual growth process) and to divide upon reaching a predetermined size. Several different methods for this more incremental domain growth description are detailed below.

A. Deterministic domain growth

Each time a particle jumps, we allow each of the intervals to grow an amount proportional to its length. This produces exponential domain growth of each interval and hence exponential domain growth of the whole domain. We allow intervals to grow to roughly (given the stochastic nature of the time stepping) twice the standard interval size (to $2\Delta x$) before dividing. Upon division, an interval splits into two equally sized daughter intervals and the particles that resided in that interval are divided randomly between these two daughter intervals using a number drawn from a binomial random variable $\mathcal{B}(n_i,0.5)$, where n_i is the number of particles in parent interval i (see Ref. [14] for further discussion of possible

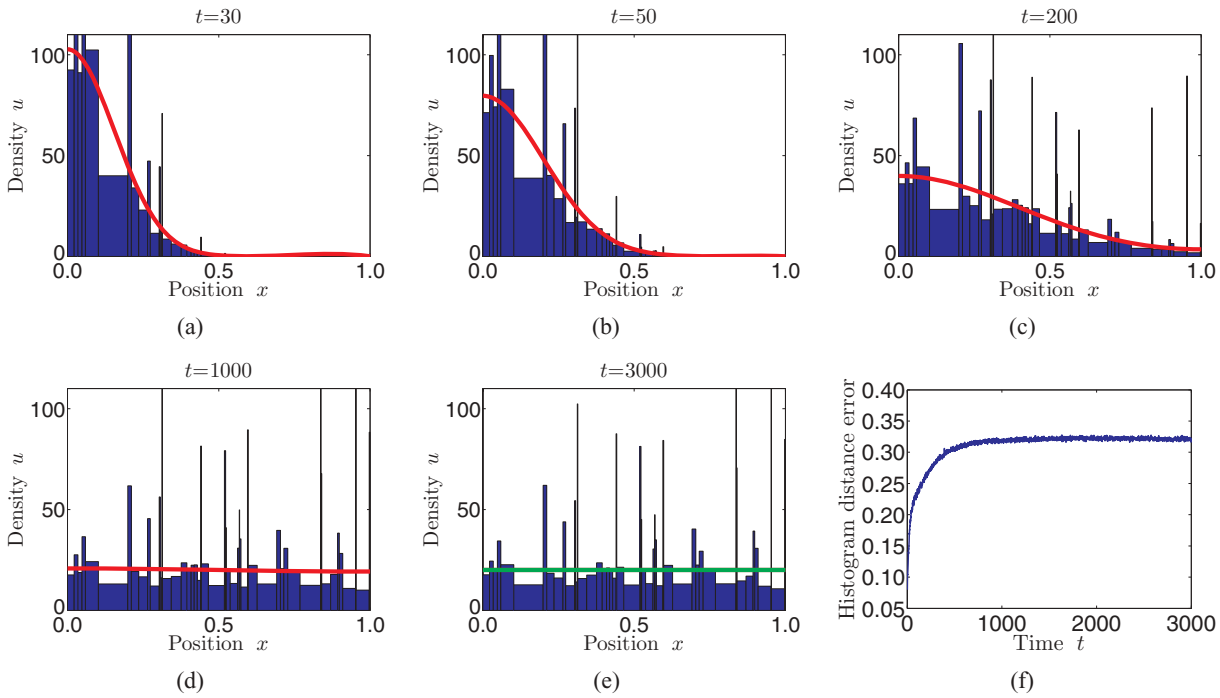

FIG. 4. (Color online) Particles undergoing simple diffusion at several time points on an interval-centered domain partition. Image descriptions and initial and boundary conditions are as in Fig. 3. With the microscopically derived transition rates, which correspond to the macroscopic PDE, the interval-centered description of diffusion leads to particle densities that do not match the mean-field description. In the panels we have cut off the tops of the histograms representing particle density so that a detailed comparison of the PDE and stochastic particle density can be made. For a video of the evolution of particle density please see movie Fig 4.avi of Ref. [17].

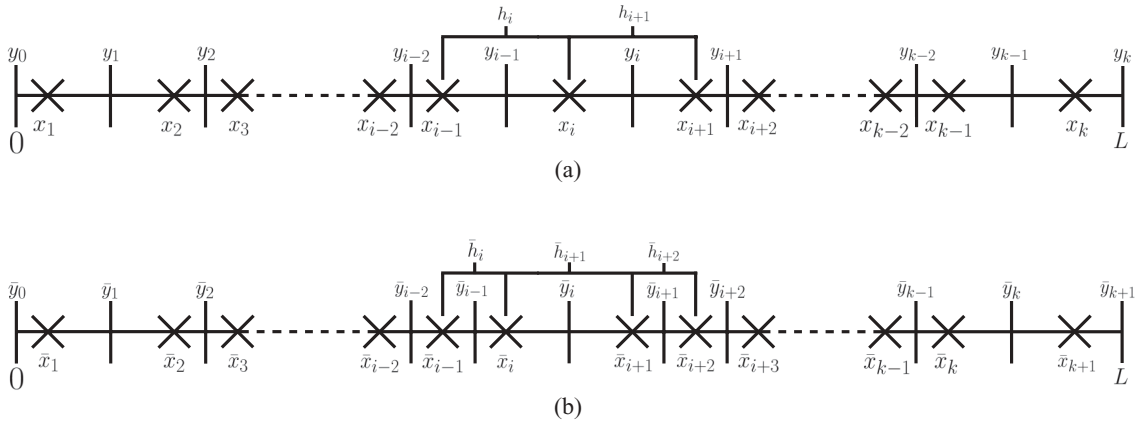

FIG. 5. Implementation of (interior) interval division while maintaining the Voronoi partition. Interval i becomes large enough to divide due to a growth event. (a) The predivision domain. (b) The domain after the division event and the consequential repartitioning of the affected intervals. It should be noted that the domain does not grow during a division event.

methods to reallocate particles into daughter intervals). We call this a division event.

Intervals initialized with the same length retain this uniformity and therefore we are not required to consider nonuniform domain partitions. Interval division will be synchronous and simple to implement.

However, allowing initial inhomogeneity requires the Voronoi partition in order to produce consistent particle densities (see Sec. S.1 of Ref. [17]). Deterministic domain growth maintains the Voronoi property of the domain and the main issue is how to appropriately repartition the domain once an interval has become large enough to divide (a division event). Ideally we would divide the parent interval into two equally sized daughter intervals, each half the length of the original parent interval. Unfortunately, in general, it is not possible to do this while maintaining the Voronoi partition. Instead it is necessary to redefine the boundaries of the two neighboring intervals of the interval that divides (see Fig. 5). We are, however, at least able to choose daughter intervals that are of equal sizes.

Begin by considering interior intervals. We can express the restriction of maintaining a Voronoi partition mathematically in terms of the positions of the predivision Voronoi point of dividing interval i, x_i, those of the two neighboring intervals x_{i-1} and x_{i+1}, and the positions of the Voronoi points after division $\bar{x}_{i-1}$, $\bar{x}_i$, $\bar{x}_{i+1}$, and $\bar{x}_{i+2}$, where we have relabeled the Voronoi points on the postdivision domain with an overbar. In order to ensure that only these three intervals are affected by the division event we must ensure that the Voronoi points x_{i-1} and x_{i+1} remain unchanged, i.e., $x_{i-1} = \bar{x}_{i-1}$ and $x_{i+1} = \bar{x}_{i+2}$. We can express the condition that the two daughter intervals should be of the same size as

$$2l = \bar{x}_{i+1} - \bar{x}_{i-1} = \bar{x}_{i+2} - \bar{x}_i, \tag{31}$$

where l is the length of the daughter intervals. We must also maintain the strict ordering of the Voronoi points:

$$\bar{x}_{i-1} < \bar{x}_i < \bar{x}_{i+1} < \bar{x}_{i+2}. \tag{32}$$

These inequalities can be shown (after manipulation) to bound the length of the daughter intervals above and below:

$$\frac{\bar{x}_{i+2} - \bar{x}_{i-1}}{4} < l < \frac{\bar{x}_{i+2} - \bar{x}_{i-1}}{2}. \tag{33}$$

Choosing the daughter intervals to be half as long as the parent interval $l = (\bar{x}_{i+2} - \bar{x}_{i-1})/4$ would mean choosing the two new Voronoi points to be coincident $\bar{x}_i = \bar{x}_{i+1}$. At the other extreme, choosing each daughter interval to be the same length as the parent interval $l = (\bar{x}_{i+2} - \bar{x}_{i-1})/2$ requires each new point to be coincident with an already existing point $\bar{x}_i = \bar{x}_{i-1}$ and $\bar{x}_{i+1} = \bar{x}_{i+2}$. Neither of these extreme situations is acceptable. An unbiased choice, therefore, would be

$$l = \tfrac{3}{8}(\bar{x}_{i+2} - \bar{x}_{i-1}). \tag{34}$$

This choice fully determines the position of the new Voronoi points (see Fig. 5):

$$\bar{x}_i = \tfrac{3}{4}\bar{x}_{i-1} + \tfrac{1}{4}\bar{x}_{i+2}, \tag{35}$$

$$\bar{x}_{i+1} = \tfrac{1}{4}\bar{x}_{i-1} + \tfrac{3}{4}\bar{x}_{i+2}. \tag{36}$$

We must be careful when dividing the end intervals. In the case of the first interval, for example, we do not need to determine the left-hand end of the interval in relation to another Voronoi point. This boundary is fixed ($\bar{y}_0 = y_0 = 0$). Clearly, we still require the ordering condition of the Voronoi points:

$$0 < \bar{x}_1 < \bar{x}_2 < \bar{x}_3. \tag{37}$$

Again the two daughter intervals are chosen to be the same size as each other, but, as an additional constraint, the first new Voronoi point $\bar{x}_1$ is chosen to lie in the center of the first interval $[\bar{y}_0, \bar{y}_1]$. This prescribes that the second Voronoi point $\bar{x}_2$ must also lie in the center of the second interval $[\bar{y}_1, \bar{y}_2]$ (since the intervals are chosen to be of the same length). This determines positions of the new Voronoi points

$$\bar{x}_1 = \frac{\bar{x}_3}{5}, \quad \bar{x}_2 = \frac{3\bar{x}_3}{5}, \tag{38}$$

and hence the repartitioning of the domain upon splitting of the first interval. In an analogous manner, when we split interval k,

the new Voronoi points must depend on the distance between the end of the domain $\bar{y}_{k+1}$ and the last unaltered Voronoi point $\bar{x}_{k-1}$ in the following way:

$$\bar{x}_k = \frac{3\bar{x}_{k-1}}{5} + \frac{2\bar{y}_{k+1}}{5}, \quad \bar{x}_{k+1} = \frac{\bar{x}_{k-1}}{5} + \frac{4\bar{y}_{k+1}}{5}. \tag{39}$$

For the purpose of particle redistribution upon splitting we assume that particles are distributed evenly across each interval. When interval boundaries are redrawn upon the splitting of interval i the number of particles in the new intervals are chosen as close as possible (given the integer nature of particle numbers) to

$$\bar{n}_{i-1} = \left(\frac{\bar{y}_{i-1} - y_{i-2}}{y_{i-1} - y_{i-2}}\right) n_{i-1}, \tag{40}$$

$$\bar{n}_i = \left(\frac{y_{i-1} - \bar{y}_{i-1}}{y_{i-1} - y_{i-2}}\right) n_{i-1} + \left(\frac{\bar{y}_i - y_{i-1}}{y_i - y_{i-1}}\right) n_i, \tag{41}$$

$$\bar{n}_{i+1} = \left(\frac{y_i - \bar{y}_i}{y_i - y_{i-1}}\right) n_i + \left(\frac{\bar{y}_{i+1} - y_i}{y_{i+1} - y_i}\right) n_{i+1}, \tag{42}$$

$$\bar{n}_{i+2} = \left(\frac{y_{i+1} - \bar{y}_{i+1}}{y_{i+1} - y_i}\right) n_{i+1}. \tag{43}$$

For each original interval j ($j = i-1, i, i+1$, where interval i is the interval chosen to split) we draw a random integer m between 0 and n_j from a binomial distribution with parameters $N = n_j$ and $p = (\bar{y}_j - y_{j-1})/(y_j - y_{j-1})$. We allow m particles to remain in new interval $\bar{j}$ and the remaining $(n_j - m)$ particles will be redistributed to new interval $\bar{j}+1$ (see Fig. 6).

On the interval-centered domain division is much simpler. A new interval boundary $\bar{y}_i$ is drawn at position x_i, the center of the interval that is dividing, and new interval centers are defined at $\bar{x}_i = (y_{i-1} + x_i)/2 = (\bar{y}_{i-1} + \bar{y}_i)/2$ and $\bar{x}_{i+1} = (y_i + x_i)/2 = (\bar{y}_i + \bar{y}_{i+1})/2$. All interval centers and edges to the right of the interval that is dividing are relabeled by increasing their index by one, i.e., $x_j = \bar{x}_{j+1}$ and $y_j = \bar{y}_{j+1}$ for $j = i+1, \ldots, k$. The n_i particles that previously resided in interval i are redistributed evenly into the two daughter intervals.

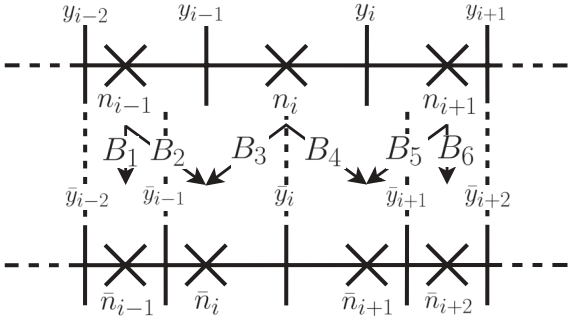

FIG. 6. Particles are redistributed after an interval divides. Each particle is redistributed to a new interval with probability proportional to the overlap between the new intervals and the old intervals using random numbers drawn from a binomial distribution: $B_1 = \mathcal{B}(n_{i-1}, (\bar{y}_{i-1} - y_{i-2})/(y_{i-1} - y_{i-2}))$, $B_2 = n_{i-1} - B_1$, $B_3 = \mathcal{B}(n_i, (\bar{y}_i - y_{i-1})/(y_i - y_{i-1}))$, $B_4 = n_i - B_3$, $B_5 = \mathcal{B}(n_{i+1}, (\bar{y}_{i+1} - y_i)/(y_{i+1} - y_i))$, and $B_6 = n_{i+1} - B_5$.

B. Stochastic domain growth

A possible alternative method for implementing domain growth is to allow intervals to grow in pairs (intervals must grow in pairs in order to preserve the Voronoi property of the domain; however, when considering the interval-centered domain partition it is possible, and indeed preferable, to allow intervals to grow individually) rather than all synchronously as described in Sec. IV A. We call this a growth event. Growth must be implemented carefully in order to preserve the Voronoi property of the domain. Intervals i and $i+1$ are chosen to grow with a probability proportional (with constant of proportionality r) to the size of interval i: $l_i = (y_i - y_{i-1})$. All the Voronoi points to the right of x_i ($x_{i+1}, \ldots, x_k$) move by a constant amount Δl to the right, where Δl is some small fraction of the standard interval length Δx. Here Δl is defined such that, when taking the continuum limit, the ratio $\Delta l/\Delta x \ll 1$ remains constant as $\Delta x \to 0$ so that terms that are of order Δl^2 may still be neglected in comparison to terms that are of order l_j, the length of the jth interval (see Sec. V C). The boundary y_i is then redrawn $\Delta l/2$ to the right of its original position. Thus growth causes intervals i and $i+1$ to grow by $\Delta l/2$ each (see Fig. 7). The only exception to this rule is for the rightmost interval of the domain where we can simply move the right-hand boundary of the interval by Δl without disturbing the Voronoi property. Upon growing to a predetermined size Δx_{split}, intervals are divided and particles redistributed in the same manner as described above. By considering a master equation for the domain length, $L(t)$, we can show that (see Sec. S.7 of Ref. [17]), on average, this process leads to exponential domain growth $L(t) = \exp(r\Delta l t)$. Crucially this growth process maintains the Voronoi property of the partition.

If we are considering an interval-centered domain partition (which may be justified in some circumstances; see Secs. S.2 and S.8 of Ref. [17]) we can implement domain growth in a much more straightforward manner. Growth of interval i occurs with rate proportional to its length l_i. Interval edges to the right of the growing interval (y_j for $j = i+1, \ldots, k$) are shifted to the right by Δl and point x_i is shifted to the right by $\Delta l/2$ in order to preserve its position in the center of interval i. Only one interval changes in size. By considering a master equation for domain length (see Sec. IV C) we can show that each interval (and hence the whole domain) grows exponentially.

C. Master equation for domain length on the interval-centered domain partition with intervals growing stochastically

In the case where intervals grow deterministically at an exponential rate it is simple to show that we arrive at the expected macroscopic PDE [see Eq. (2)] for particle density (see Sec. S.3 of Ref. [17]). We instead focus on deriving a PDE for particle density in the case of stochastic growth. For ease of working we consider the interval-centered domain partition, although we can also derive similar results for the Voronoi partition (see Sec. S.7 of Ref. [17]). The interval-centered partition admits the possibility of individual interval growth with rate proportional to interval length and simple interval division. In addition, it is possible to repartition the interval-centered domain in order to calculate the particle densities that correspond to the mean-field PDE and as such

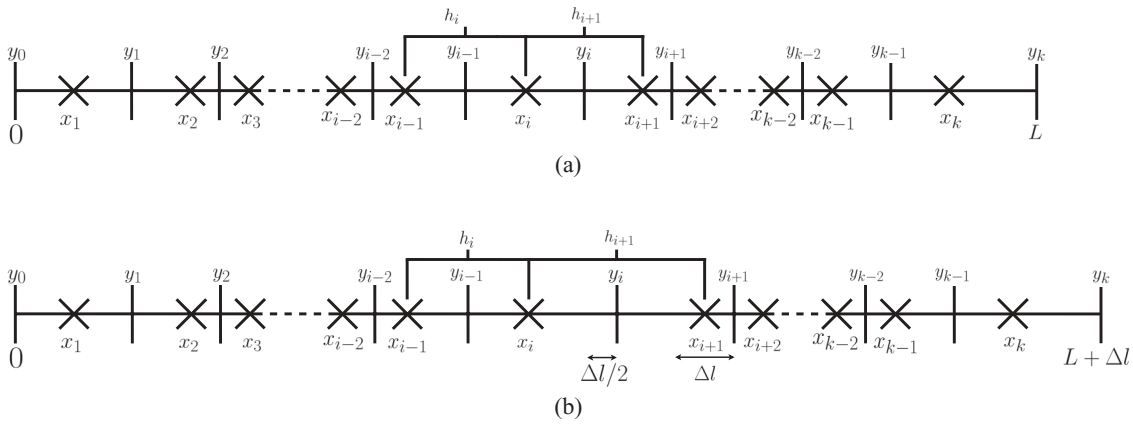

FIG. 7. Implementation of individual domain growth on the Voronoi domain partition. Interval i is selected to grow with probability proportional to its length l_i. (a) The pregrowth domain. (b) The domain after the implementation of the growth of intervals i and $i+1$, each by $\Delta l/2$ as described above.

the interval-centered domain partition may be as valid as the Voronoi domain partition for simulating particle migration on growing domains (see Sec. S.8 of Ref. [17]).

Consider a time interval small enough that the probability of more than one growth event occurring in $[t,t+\delta t)$ is $O(\delta t)$ and ignore, for the meantime, the movement of particles. Define $\boldsymbol{L}=(L_1,\ldots,L_k)$ to be the vector of random variables representing the length of each interval. We express the probability that the jth component of $\boldsymbol{L}$, representing the length of interval j, takes the value l_j at time $t+\delta t$ via the following master equation:

$$\frac{\partial \text{Prob}(\boldsymbol{L}=\boldsymbol{l},t)}{\partial t} = r\sum_{i=1}^{k}\text{Prob}(\boldsymbol{L}=(l_1,\ldots,l_i-\Delta l,\ldots,l_k),t) \times (l_i-\Delta l) - r\sum_{i=1}^{k} l_i \text{Prob}(\boldsymbol{L}=\boldsymbol{l},t), \tag{44}$$

where $\boldsymbol{l}=(l_1,\ldots,l_k)$ is the current state of the vector of interval length random variables. In order to find the mean length of interval j we multiply through by l_j and sum over all the (finite number of) possible values that $\boldsymbol{l}$ can take. Upon simplification we arrive at an ordinary differential equation (ODE) that describes how the mean length of each interval changes:

$$\frac{d\langle l_j\rangle}{dt} = r\Delta l\langle l_j\rangle \quad \text{for} \quad j=1,\ldots,k \tag{45}$$

$$\Rightarrow \langle l_j\rangle(t) = l_j(0)\exp(r\Delta l t) \quad \text{for} \quad j=1,\ldots,k, \tag{46}$$

where $l_j(0)$ is the initial size of interval j. By taking the sum of ODEs (45) we can arrive at an ODE for the average domain length $\langle L\rangle$:

$$\frac{d\langle L\rangle}{dt} = r\Delta l\langle L\rangle \tag{47}$$

$$\Rightarrow \langle L\rangle(t) = L(0)\exp(r\Delta l t), \tag{48}$$

where $L(0)=\sum_{j=1}^{k} l_j(0)$ is the original length of the domain.

Although, using the Voronoi domain partition, the average domain length $\langle L\rangle$ can be shown to grow exponentially, each individual interval cannot grow exponentially. This is because interval i grows as a result of a growth event with probability proportional to its length l_i or as a result of a growth event with probability proportional to l_{i-1}. This means that the rate of growth for each interval is dependent on its current length, but also on the length of its leftmost neighbor, which excludes the possibility of exponential growth of individual intervals (see Sec. S.7.1 of Ref. [17] for a derivation of interval growth rates on the Voronoi partition [17]).

V. DERIVATION OF THE PARTIAL DIFFERENTIAL EQUATION FOR GROWTH FROM THE MASTER EQUATION

First we introduce some notation: ρ_j will denote the density of particles in interval j after the growth event and N_j will denote the number of particles in interval j after the growth event (which will be the same as the number of particles in interval j before the growth event since growth events do not change the number of particles in each interval). In addition, l_j will denote the postgrowth length of interval j. Clearly these three quantities are related by

$$\rho_j = \frac{N_j}{l_j} \tag{49}$$

for each postgrowth interval j.

A. Conceptual point

Since we have defined ρ_j as being the density of particles in interval j on the postgrowth domain, it is important that we express all other terms pertaining to particles density in terms of densities on the postgrowth domain. As such we would like to repartition the pregrowth particle densities from the pregrowth domain partition to the postgrowth domain partition.

B. Pregrowth densities on the postgrowth domain partition

To repartition particles from the pregrowth domain to the postgrowth domain we must first repartition the pregrowth particle numbers on the pregrowth domain partition, denoted

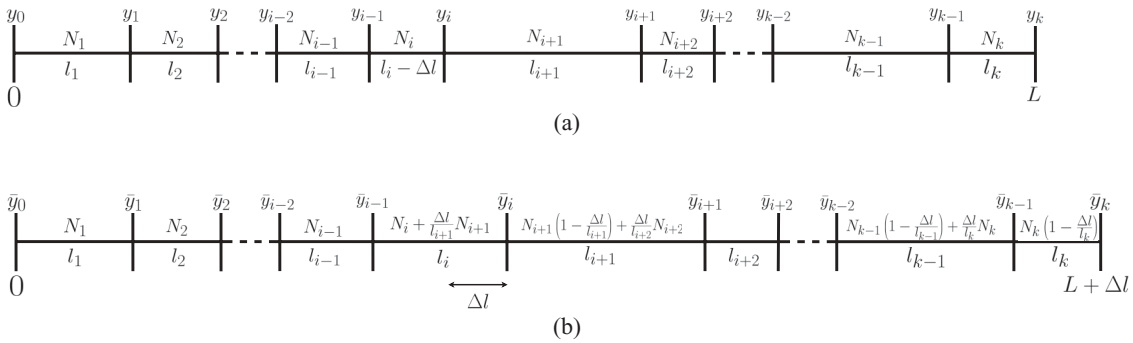

FIG. 8. Pregrowth particle numbers partitioned on (a) the pregrowth domain and (b) the postgrowth domain. The number of particles in each interval is given in the upper half of each interval and the length of that interval is given in the lower half. Repartitioning the particle numbers as in (b) allows us to easily write the pregrowth particle densities on the postgrowth domain partition.

by the vector $\boldsymbol{N}$, to the postgrowth domain partition. This repartitioned vector will be denoted $\boldsymbol{N}'$. Since the pre- and postgrowth domain partitions are the same up to the interval i, which grows, we have $N'_j = N_j$ for $j < i$. Since interval i grows, the number of particles in the pregrowth domain that lie in the postgrowth interval i is $N'_i = N_i + N_{i+1}\Delta l/l_{i+1}$. This corresponds to all the particles that lie in the pregrowth interval i added to the fraction $\Delta l/l_{i+1}$ of the particles that lie in the pregrowth interval $i+1$, N_{i+1}. This fraction $(\Delta l/l_{i+1})$ is the amount of overlap between the postgrowth interval i and the pregrowth interval $i+1$ and our repartitioning assumes particles are spread homogeneously across each interval. In a similar manner, the number of particles in the pregrowth domain that lie in postgrowth interval $j > i$ is $N'_j = N_j(1 - \Delta l/l_j) + (\Delta l/l_{j+1})N_{j+1}$. The factor $\Delta l/l_j$ corresponds to the fraction of particles in pregrowth interval j lost to postgrowth interval $j-1$ (hence $1 - \Delta l/l_j$ corresponds to the fraction of particles in pregrowth interval j that are also in postgrowth interval j). Correspondingly $\Delta l/l_{j+1}$ is the number of particles requisitioned by postgrowth interval j from pregrowth interval $j+1$ (see Fig. 8). Finally, the number of particles that lie in postgrowth interval k is $N'_k = N_k(1 - \Delta l/l_k)$, where $1 - \Delta l/l_k$ represents the overlap fraction of pre- and postgrowth intervals k.

Now that we have repartitioned the particle numbers to the postgrowth domain partition, it is a simple matter to find the pregrowth densities on the postgrowth domain partition q_j. For all $j < i$ we have

$$q_j = \frac{N_j}{l_j} = \rho_j, \tag{50}$$

since the boundaries of these intervals are the same on the post- and pregrowth domain partition (see Fig. 8). For $j = i$,

$$q_i = \frac{N_i + N_{i+1}(\Delta l/l_{i+1})}{l_i} = \rho_i + \frac{\Delta l}{l_i}\rho_{i+1}. \tag{51}$$

Similarly, if $i < j < k$ then we can write the pregrowth densities on the postgrowth domain partition q_j associated with interval j as

$$\begin{aligned} q_j &= \frac{N_j(1 - \Delta l/l_j) + (\Delta l/l_{j+1})N_{j+1}}{l_j} \\ &= \rho_j(1 - \Delta l/l_j) + \frac{\Delta l}{l_j}\rho_{j+1}. \end{aligned} \tag{52}$$

Finally, for the last interval k the density will become

$$q_k = \frac{N_k(1 - \Delta l/l_k)}{l_k} = \rho_k(1 - \Delta l/l_k). \tag{53}$$

C. Master equation

Now that we have formulated the pregrowth densities q_j in terms of the postgrowth densities ρ_j on the postgrowth grid we are in a position to consider the master equation for domain growth. Consider the probability of having particle density vector $\boldsymbol{\rho}$ and interval length vector $\boldsymbol{l}$ at time $t + \delta t$, where the time increment δt is small enough that the probability of more than one growth event occurring is $O(\delta t)$. Ignoring, for the meantime, particle movement and the effects of signal sensing and considering all the possible ways we could have arrived in this state space from time t provides us with a formulation of the master equation for particle density on a growing domain:

$$\begin{aligned} \frac{\partial \mathrm{Prob}(\boldsymbol{\rho},\boldsymbol{l},t)}{\partial t} &= r\sum_{i=1}^{k} \mathrm{Prob}(q_1,\ldots,q_i,q_{i+1},\ldots,q_k,l_1, \\ &\quad \ldots,l_i - \Delta l,\ldots,l_k,t)(l_i - \Delta l) \\ &\quad - r\sum_{i=1}^{k} \mathrm{Prob}(\boldsymbol{\rho},\boldsymbol{l},t)l_i. \end{aligned} \tag{54}$$

Multiplying through by the particle density in interval j, ρ_j, and summing over all the possible values that the particle density can take, we arrive at

$$\begin{aligned} \frac{d\langle\rho_j\rangle}{dt} &= r\sum_{i=1}^{k}\sum_{\boldsymbol{\rho}} \rho_j \mathrm{Prob}(q_1,\ldots,q_i,q_{i+1},\ldots,q_k,l_1, \\ &\quad \ldots,l_i - \Delta l,\ldots,l_k,t)(l_i - \Delta l) - r\sum_{i=1}^{k}\langle\rho_j l_i\rangle, \end{aligned} \tag{55}$$

where $\langle\rho_j\rangle = \sum_{\boldsymbol{\rho}} \rho_j \mathrm{Prob}(\boldsymbol{\rho},\boldsymbol{l},t)$ represents the mean number of particles in interval j and $\langle\rho_j l_i\rangle = \sum_{\boldsymbol{\rho}} \rho_j l_i \mathrm{Prob}(\boldsymbol{\rho},\boldsymbol{l},t)$. Note that values that the particle density can take are determined by the number of particles in the interval and the width of that interval. Therefore, in the above equation and elsewhere, we use the shorthand notation $\sum_{\boldsymbol{\rho}}$ to represent the

double sum over all possible particle numbers and all possible interval widths $\sum_{\boldsymbol{N}} \sum_{\boldsymbol{l}}$. For the first sum on the right-hand side of Eq. (55) we must carefully consider each value of i. For $i > j$ the terms are of the form

$$r \sum_{\boldsymbol{\rho}} \rho_j \text{Prob}(q_1, \ldots, q_i, q_{i+1}, \ldots, q_k, l_1, \ldots, l_i - \Delta l, \ldots, l_k, t)(l_i - \Delta l) = r \langle \rho_j l_i \rangle \tag{56}$$

since $q_j = \rho_j$ for $j < i$. However, if $i \leqslant j$ then the growth event occurs at, or to the left of, interval j and things are not so simple.

For $j = i$,

$$\begin{aligned}
&r \sum_{\boldsymbol{\rho}} \rho_j \text{Prob}\Big(\rho_1, \ldots, \rho_{j-1}, \rho_j + \frac{\Delta l}{l_j}\rho_{j+1}, \rho_{j+1}\Big(1 - \frac{\Delta l}{l_{j+1}}\Big) + \frac{\Delta l}{l_{j+1}}\rho_{j+2}, \ldots, \rho_k(1 - \Delta l/l_k), l_1, \ldots, l_j - \Delta l, \ldots, l_k, t\Big)(l_j - \Delta l) \\
&\quad = r \sum_{\boldsymbol{\rho}} \Big(\rho_j + \frac{\Delta l}{l_j}\rho_{j+1}\Big)\text{Prob}\Big(\rho_1, \ldots, \rho_{j-1}, \rho_j + \frac{\Delta l}{l_j}\rho_{j+1}, \rho_{j+1}\Big(1 - \frac{\Delta l}{l_{j+1}}\Big) \\
&\qquad + \frac{\Delta l}{l_{j+1}}\rho_{j+2}, \ldots, \rho_k(1 - \Delta l/l_k), l_1, \ldots, l_j - \Delta l, \ldots, l_k, t\Big)(l_j - \Delta l) \\
&\qquad - r \sum_{\boldsymbol{\rho}} \frac{\Delta l}{l_j}\rho_{j+1}\text{Prob}\Big(\rho_1, \ldots, \rho_{j-1}, \rho_j + \frac{\Delta l}{l_j}\rho_{j+1}, \rho_{j+1}\Big(1 - \frac{\Delta l}{l_{j+1}}\Big) \\
&\qquad + \frac{\Delta l}{l_{j+1}}\rho_{j+2}, \ldots, \rho_k(1 - \Delta l/l_k), l_1, \ldots, l_j - \Delta l, \ldots, l_k, t\Big)(l_j - \Delta l) \\
&\quad = r\langle \rho_j l_j \rangle - r \sum_{\boldsymbol{\rho}} \frac{\Delta l}{l_j}\Big(\frac{l_{j+1}}{l_{j+1} - \Delta l}\Big)\Big\{\rho_{j+1}\Big(1 - \frac{\Delta l}{l_{j+1}}\Big) + \frac{\Delta l}{l_{j+1}}\rho_{j+2}\Big\}\text{Prob}\Big(\rho_1, \ldots, \rho_{j-1}, \rho_j + \frac{\Delta l}{l_j}\rho_{j+1}, \rho_{j+1}\Big(1 - \frac{\Delta l}{l_{j+1}}\Big) \\
&\qquad + \frac{\Delta l}{l_{j+1}}\rho_{j+2}, \ldots, \rho_k(1 - \Delta l/l_k), l_1, \ldots, l_j - \Delta l, \ldots, l_k, t\Big)(l_j - \Delta l) + O(\Delta l^2) \\
&\quad = r\langle \rho_j l_j \rangle - r\Delta l \langle \rho_{j+1} \rangle + O(\Delta l^2).
\end{aligned} \tag{57}$$

To go between the first and second equalities in this statement we have added and subtracted terms that are $O(\Delta l^2)$, namely,

$$r \sum_{\boldsymbol{\rho}} \frac{\Delta l}{l_j}\Big(\frac{l_{j+1}}{l_{j+1} - \Delta l}\Big)\frac{\Delta l}{l_{j+1}}\rho_{j+2}\text{Prob}(\cdots)(l_j - \Delta l), \tag{58}$$

where the term we have added is incorporated into the $O(\Delta l^2)$ term. To go between the second and third equalities we have used the Taylor expansion of $1/(l_{j+1} - \Delta l)$ and grouped all $O(\Delta l^2)$ terms together:

$$\frac{1}{l_{j+1} - \Delta l} = \frac{1}{l_{j+1}} + \frac{\Delta l}{(l_{j+1})^2} + O(\Delta l^2), \tag{59}$$

so that $\Delta l(l_{j+1}/(l_{j+1} - \Delta l))$ may be approximated by $\Delta l + O(\Delta l^2)$. We have also made use of the following Taylor expansion of $1/l_j$:

$$\frac{1}{l_j} = \frac{1}{(l_j - \Delta l) + \Delta l} = \frac{1}{l_j - \Delta l} - \frac{\Delta l}{(l_j - \Delta l)^2} + O(\Delta l^2), \tag{60}$$

so that $\Delta l/l_j$ may be approximated as $\Delta l/\left(l_j - \Delta l\right) + O(\Delta l^2)$.

In general, for $1 \leqslant i < j$ all terms will take a similar form

$$\begin{aligned}
&r \sum_{\boldsymbol{\rho}} \rho_j \text{Prob}\Big(q_1, \ldots, q_{j-1}, \rho_j(1 - \Delta l/l_j) + \frac{\Delta l}{l_j}\rho_{j+1}, \rho_{j+1}(1 - \Delta l/l_{j+1}) \\
&\qquad + \frac{\Delta l}{l_{j+1}}\rho_{j+2}, \ldots, \rho_k(1 - \Delta l/l_k), l_1, \ldots, l_i - \Delta l, \ldots, l_k, t\Big)(l_i - \Delta l) \\
&\quad = r \sum_{\boldsymbol{\rho}} \Big(\frac{l_j}{l_j - \Delta l}\Big)\Big(\rho_j(1 - \Delta l/l_j) + \frac{\Delta l}{l_j}\rho_{j+1}\Big)\text{Prob}\Big(q_1, \ldots, q_{j-1}, \rho_j(1 - \Delta l/l_j) + \frac{\Delta l}{l_j}\rho_{j+1}, \rho_{j+1}(1 - \Delta l/l_{j+1}) \\
&\qquad + \frac{\Delta l}{l_{j+1}}\rho_{j+2}, \ldots, \rho_k(1 - \Delta l/l_k), l_1, \ldots, l_i - \Delta l, \ldots, l_k, t\Big)(l_i - \Delta l)
\end{aligned}$$

$$
\begin{aligned}
&- r\sum_{\boldsymbol{\rho}}\left(\frac{\Delta l}{l_j-\Delta l}\right)\rho_{j+1}\mathrm{Prob}\Big(q_1,\ldots,q_{j-1},\rho_j(1-\Delta l/l_j)+\frac{\Delta l}{l_j}\rho_{j+1},\rho_{j+1}(1-\Delta l/l_{j+1})\\
&+\frac{\Delta l}{l_{j+1}}\rho_{j+2},\ldots,\rho_k(1-\Delta l/l_k),l_1,\ldots,l_i-\Delta l,\ldots,l_k,t\Big)(l_i-\Delta l)\\
&=r\sum_{\boldsymbol{\rho}}\left(1+\frac{\Delta l}{l_j-\Delta l}\right)\Big(\rho_j(1-\Delta l/l_j)+\frac{\Delta l}{l_j}\rho_{j+1}\Big)\mathrm{Prob}\Big(q_1,\ldots,q_{j-1},\rho_j(1-\Delta l/l_j)\\
&+\frac{\Delta l}{l_j}\rho_{j+1},\rho_{j+1}(1-\Delta l/l_{j+1})+\frac{\Delta l}{l_{j+1}}\rho_{j+2},\ldots,\rho_k(1-\Delta l/l_k),l_1,\ldots,l_i-\Delta l,\ldots,l_k,t\Big)(l_i-\Delta l)\\
&-r\sum_{\boldsymbol{\rho}}\left(\frac{\Delta l}{l_j-\Delta l}\right)\left(\frac{l_{j+1}}{l_{j+1}-\Delta l}\right)\left\{\rho_{j+1}\left(1-\frac{\Delta l}{l_{j+1}}\right)+\frac{\Delta l}{l_{j+1}}\rho_{j+2}\right\}\mathrm{Prob}\Big(q_1,\ldots,q_{j-1},\rho_j(1-\Delta l/l_j)\\
&+\frac{\Delta l}{l_j}\rho_{j+1},\rho_{j+1}(1-\Delta l/l_{j+1})+\frac{\Delta l}{l_{j+1}}\rho_{j+2},\ldots,\rho_k(1-\Delta l/l_k),l_1,\ldots,l_i-\Delta l,\ldots,l_k,t\Big)(l_i-\Delta l)+O(\Delta l^2)\\
&=r\langle\rho_j l_i\rangle+r\Delta l\left\langle\frac{\rho_j l_i}{l_j}\right\rangle-r\Delta l\left\langle\frac{\rho_{j+1}l_i}{l_j}\right\rangle+O(\Delta l^2).
\end{aligned}
\tag{61}
$$

Again, to arrive at the last equality we have used a Taylor expansion of $1/(l_j-\Delta l)$,

$$
\frac{1}{l_j-\Delta l}=\frac{1}{l_j}+\Delta l\frac{1}{(l_j)^2}+O(\Delta l^2), \tag{62}
$$

and the Taylor expansion of $1/(l_{j+1}-\Delta l)$ from the case $i=j$ above. We substitute the expressions from Eqs. (56), (57), and (61) into the right-hand side of the master equation (55):

$$
\begin{aligned}
\frac{\partial\langle\rho_j\rangle}{\partial t}&=r\sum_{i=1}^{k}\langle\rho_j l_i\rangle-r\sum_{i=1}^{k}\langle\rho_j l_i\rangle+r\Delta l\sum_{i=1}^{j-1}\left\langle\frac{\rho_j l_i}{l_j}\right\rangle\\
&\quad-\left\langle\frac{\rho_{j+1}l_i}{l_j}\right\rangle+r\Delta l\left\langle\frac{\rho_j l_j}{l_j}\right\rangle-r\Delta l\left\langle\frac{\rho_{j+1}l_j}{l_j}\right\rangle\\
&\quad-r\Delta l\langle\rho_j\rangle+O(\Delta l^2),
\end{aligned}
\tag{63}
$$

where we have added and subtracted $r\Delta l\langle\rho_j l_j/l_j\rangle=r\Delta l\langle\rho_j\rangle$ to the right-hand side. This can be written more simply as

$$
\frac{\partial\langle\rho_j\rangle}{\partial t}=-r\Delta l\langle\rho_j\rangle-r\Delta l\sum_{i=1}^{j}\left(\left\langle\frac{\rho_{j+1}l_i}{l_j}\right\rangle-\left\langle\frac{\rho_j l_i}{l_j}\right\rangle\right). \tag{64}
$$

We make a moment closure approximation in order to make these terms manageable. To do this we assume

$$
\left\langle\frac{\rho_j l_i}{l_j}\right\rangle=\frac{\langle\rho_j\rangle\langle l_i\rangle}{\langle l_j\rangle}. \tag{65}
$$

We justify the use of this moment closure approximation using numerical simulations in Sec. VI C. Upon applying this moment closure approximation we can rewrite Eq. (64) as

$$
\frac{\partial\langle\rho_j\rangle}{\partial t}=-r\Delta l\langle\rho_j\rangle-xr\Delta l\frac{\langle\rho_{j+1}\rangle-\langle\rho_j\rangle}{\langle l_j\rangle}, \tag{66}
$$

where we have recognized that $\sum_{i=1}^{j}\langle l_i\rangle=x$. Taylor expanding the term ρ_{j+1} and taking the limit of the interval sizes tending to zero (note that in order to maintain a constant rate of domain growth, as $l_j\to 0$, we allow $\Delta l\to 0$ in such a way that $r\Delta l$ remains constant), i.e. $l_j\to 0$, yields a PDE formulation

$$
\frac{\partial u}{\partial t}=D\frac{\partial^2 u}{\partial x^2}-r\Delta l u-xr\Delta l\frac{\partial u}{\partial x}, \tag{67}
$$

for particle density $u=u(x,t)$, where we have reintroduced terms due to particle movement since their inclusion does not affect the derivation of the domain growth terms.

These are precisely the terms we would expect, as per Eq. (2), when considering exponential domain growth. The term $r\Delta l\langle\rho_j\rangle$ corresponds to local dilution due to volume increase and $xr\Delta l\partial\langle\rho_j\rangle/\partial x$ corresponds to material being transported along the domain by the flow induced by growth.

Here we have derived a PDE for the mean density $\langle\rho_j\rangle=\langle N_j/l_j\rangle$. It should be noted that it may be simpler to derive a PDE for the mean number of particles in each interval divided by the mean interval length $\langle N_j\rangle/\langle l_j\rangle$, which can in some senses be thought to be the mean density. Such a derivation for the interval-centered domain partition is given in Sec. S.3 of Ref. [17]).

The derivation of the PDE on the Voronoi domain is similar to that of the PDE on the interval-centered domain partition, illustrated above, and is given in Sec. S.7.2 of Ref. [17]). As we have already hinted, the PDE derived for the Voronoi domain partition is similar to, but not exactly the same as, the PDE derived above for the interval-centered partition. This is because the domain growth is not uniformly exponential across each interval of the Voronoi domain partition.

VI. NUMERICAL SIMULATIONS

To corroborate our findings we have carried out extensive numerical simulations using different domain growth mechanisms and interval partitions. We note the difficulty in representing average particle densities over several repeats: In the stochastic implementations of domain growth the partition of the domain in each of the repeat simulations will be different. In the deterministic implementations of domain growth (see

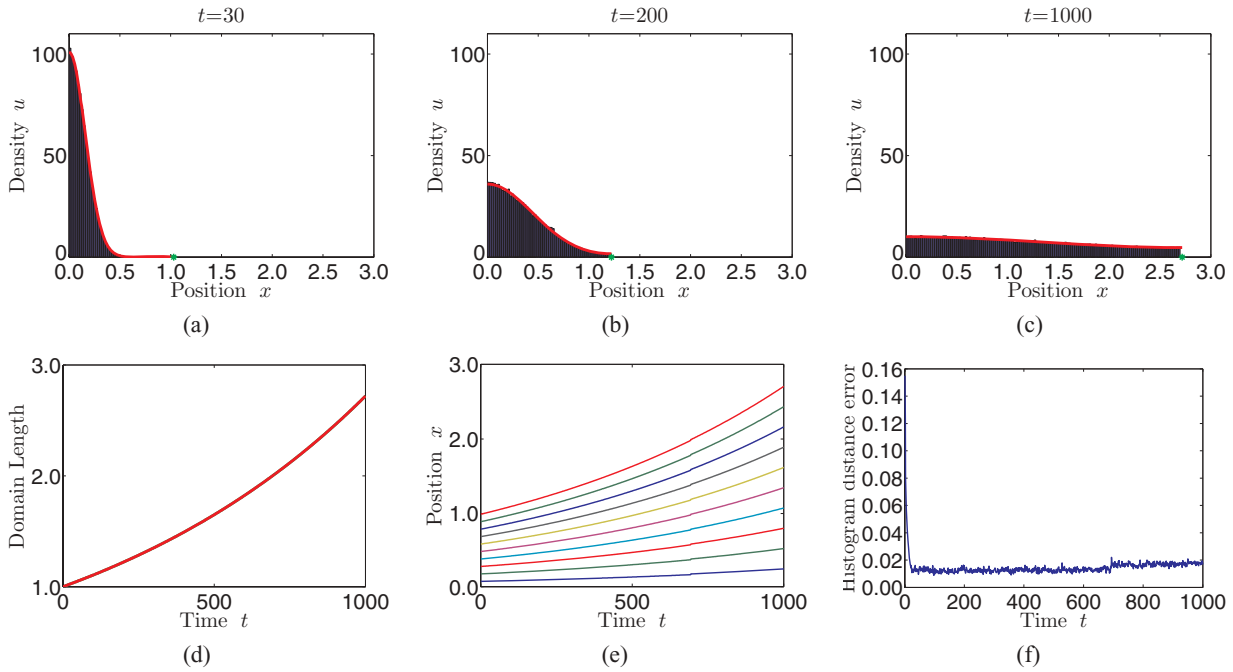

FIG. 9. (Color online) Particles undergoing diffusion at several time points. (a)–(c) The histograms represent an average of 40 stochastic realizations. The underlying individual-based model has an initially uniform domain partition and undergoes deterministic growth. The solid red (dark gray) lines exhibit the result of numerical simulation of the corresponding diffusion equation on an exponentially growing domain using the NAG routine D03PE as outlined in Sec. S.4 of Ref. [17]. The boundaries are assumed to be reflecting. The green (light gray) dot on the x axis represents the average stochastic domain length. (d) Evolution of the average stochastic domain length plotted in green (light gray) with the deterministic PDE domain length overlaid in red (dark gray). Due to the deterministic implementation of domain growth in the stochastic model, the green (light gray) curve lies exactly underneath the red curve and cannot be seen. (e) The progression of every fifth interval of the initial 50. Upon division we track the rightmost of the daughter intervals. The lines indicate the trajectories of these intervals. (f) Evolution of the histogram distance error with time (as described in Sec. III B). All particles are initialized in the first interval. Parameters are as follows: $k_0 = 50$, $\Delta x = 1/k_0 = 0.02$, $D = \Delta x^2$, $r = 0.0001$, and $\Delta x_{\text{split}} = 2\Delta x = 0.04$. For a video of the evolution of particle density and domain length please see movie Fig 9.avi of Ref. [17].

Sec. IV A) all the intervals grow at the same rate, implying that the domain partition should be the same at all the sampled time points. However, due to the stochastic nature of the particle movement and the time step chosen for each reaction, simulations cannot be sampled with exactly the same domain partition. These factors require us to rethink what we mean by average particle density. To circumvent this problem we define a uniform mesh over the domain and redistribute particle density into these regions at time points where we wish to record the density. This relies on the assumption that particles are spread homogeneously across each interval.

A. Particles diffusing on an initially uniform domain partition with deterministic exponential interval growth

In Fig. 9 we implement deterministic domain growth on an initially uniform domain partition, as described in Sec. IV A. In this case the interval-centered and Voronoi domain partitions are equivalent. Particle densities in both the stochastic and PDE models are found to match well, as evidenced quantitatively by the evolution of the histogram distance error with time [see Fig. 9(f)]. Note that in all the histogram distance error figures in this paper, when particles are initialized in the first interval the error starts off large as an artifact of the way we are forced to initialize our PDE to replicate this condition. When we initialize with an exponentially decaying profile of particles (see Fig. S.1 in Ref. [17], for example) we do not see this initial disparity since this initial profile is straightforward to replicate in the continuum model.

The domain in the individual-level model grows, on average, at the same rate as the domain of the population-level model, as exhibited in Fig. 9(d). This is what we expect for the deterministic implementation of domain growth. In Fig. 9(e) each interval tracked progresses in an exponential manner as the domain grows. A slight jump is seen at around $t \approx 700$ when all the boxes divide simultaneously and we continue to track the rightmost of the daughter intervals. The histogram distance error in Fig. 9(f) is low and remains so for the duration of the simulation. For all the numerical simulations presented in this section we have found that the histogram distance error is at least as small as its counterpart simulated using the instantaneous interval splitting and doubling of Baker *et al.* [14] (see Fig. S.3 in Sec. S.5 of Ref. [17]). In some cases it is significantly lower, especially later in simulations when a large number of interval division events has occurred.

B. Particles diffusing on an initially nonuniform domain partition with stochastic interval growth

In Fig. 10 we implement stochastic domain growth on an initially nonuniform Voronoi domain partition, as described in Secs. IV A and IV B. The average stochastic domain grows

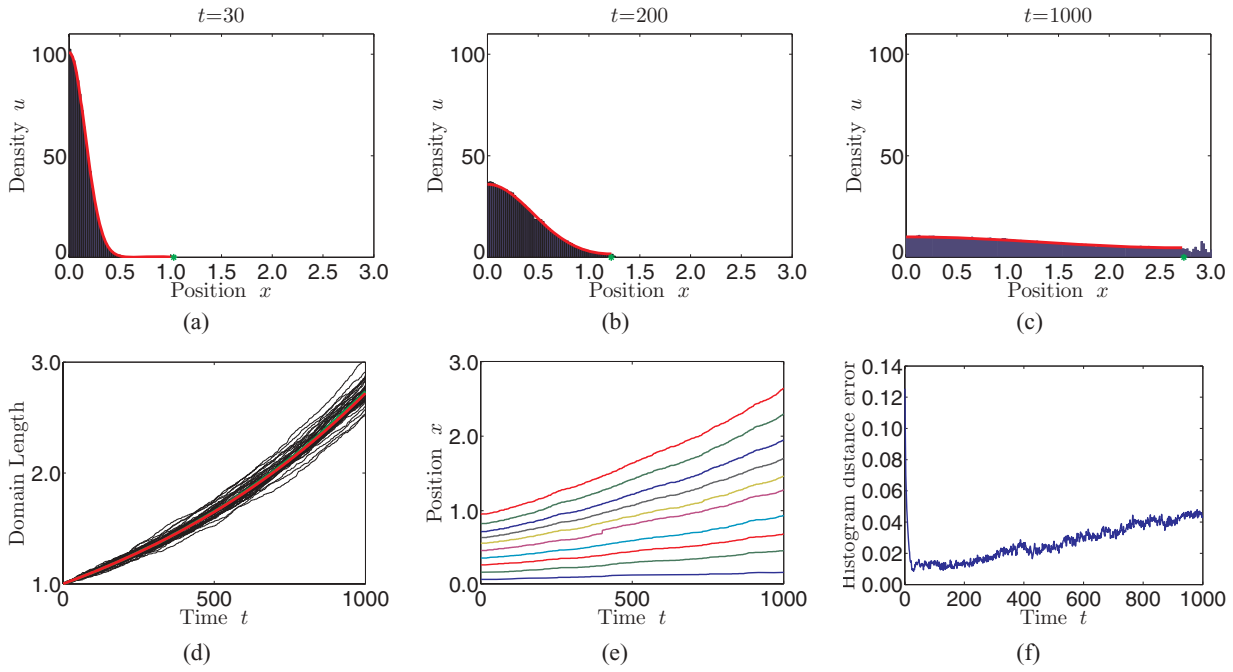

FIG. 10. (Color online) Particles undergoing diffusion at several time points. The underlying stochastic model has an initially nonuniform Voronoi domain partition and undergoes stochastic interval growth. Figure descriptions are as in Fig. 9. In (d) we can now just make out the green (light gray) curve representing evolution of the average stochastic domain length. All particles are initialized in the first interval. Parameters are as in Fig. 9 with $\Delta l = 0.1 \times \Delta x = 0.002$ in addition. For a video of the evolution of particle density and domain length please see movie Fig. 10.avi of Ref. [17].

at a rate similar to the deterministic domain, as exhibited in Fig. 10(d). This also shows the variation in the individual realizations of the stochastic domain. Both the deterministic and stochastic domains exhibit exponential growth, as expected. In Fig. 10(e) each interval tracked progresses in an exponential manner as the domain grows with occasional jumps relating

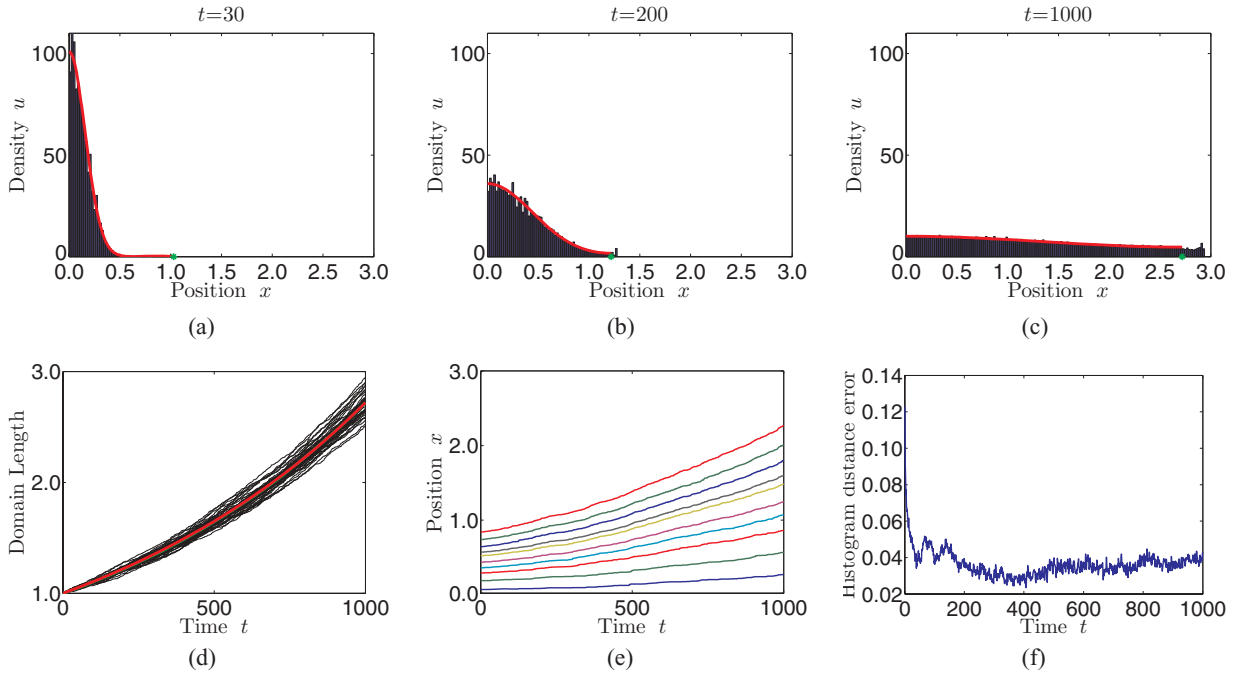

FIG. 11. (Color online) Particles undergoing diffusion at several time points. The underlying stochastic model has an initially nonuniform interval-centered domain partition and undergoes stochastic interval growth. All repeats are initialized with the same domain partition. Figure descriptions are as in Figs. 9 and 10. All particles are initialized in the first interval. Parameters are as in Fig. 10. For a video of the evolution of particle density and domain length please see movie Fig. 11.avi of Ref. [17].

to interval division events. The evolution of the histogram distance error with time [see Fig. 10(f)] demonstrates the similarity of the two model types throughout the simulations.

For comparison, in Fig. 11 we show the stochastic evolution of particle density on an initially nonuniform interval-centered domain partition. For each repeat of the simulation the same initial partition is used. The stochastic particle density gives a fair comparison to the PDE, but there are clearly discrepancies in the particle density at several points. The randomness of the growth process ensures a smoothing of the average stochastic particle density, which is why the differences between the stochastic and continuum models are not as stark as in the case of the interval-centered partition on the stationary domain. However, if the initial partitions are different for each repeat of the stochastic simulation we see that the stochastic particle density is an even better match to the PDE and the histogram distance error is correspondingly reduced (see Fig. S.4 of Ref. [17]). The behavior of the system averaged over many repeats is different from the behavior we would expect to see from a single simulation. A related phenomenon has also been observed when modeling exclusion processes for discrete agents undergoing random walks on a two-dimensional lattice [3,21]. Although the interval-centered domain partition appears to perform quite well, the Voronoi domain partition has a lower histogram distance error throughout due to the erroneous calculation of the particle densities for each of the individual simulations on the interval-centered domain partition.

C. Justification of the moment closure approximation

In order to derive the equivalence between the stochastic and continuum descriptions of particle migration it is necessary to make the moment closure approximation of Eq. (65). We attempt to justify this moment closure approximation using the results of our stochastic simulations by plotting

$$\left(\left\langle \frac{\rho_j l_i}{l_j} \right\rangle - \frac{\langle \rho_j \rangle \langle l_i \rangle}{\langle l_j \rangle}\right) \Big/ \left\langle \frac{\rho_j l_i}{l_j} \right\rangle, \tag{68}$$

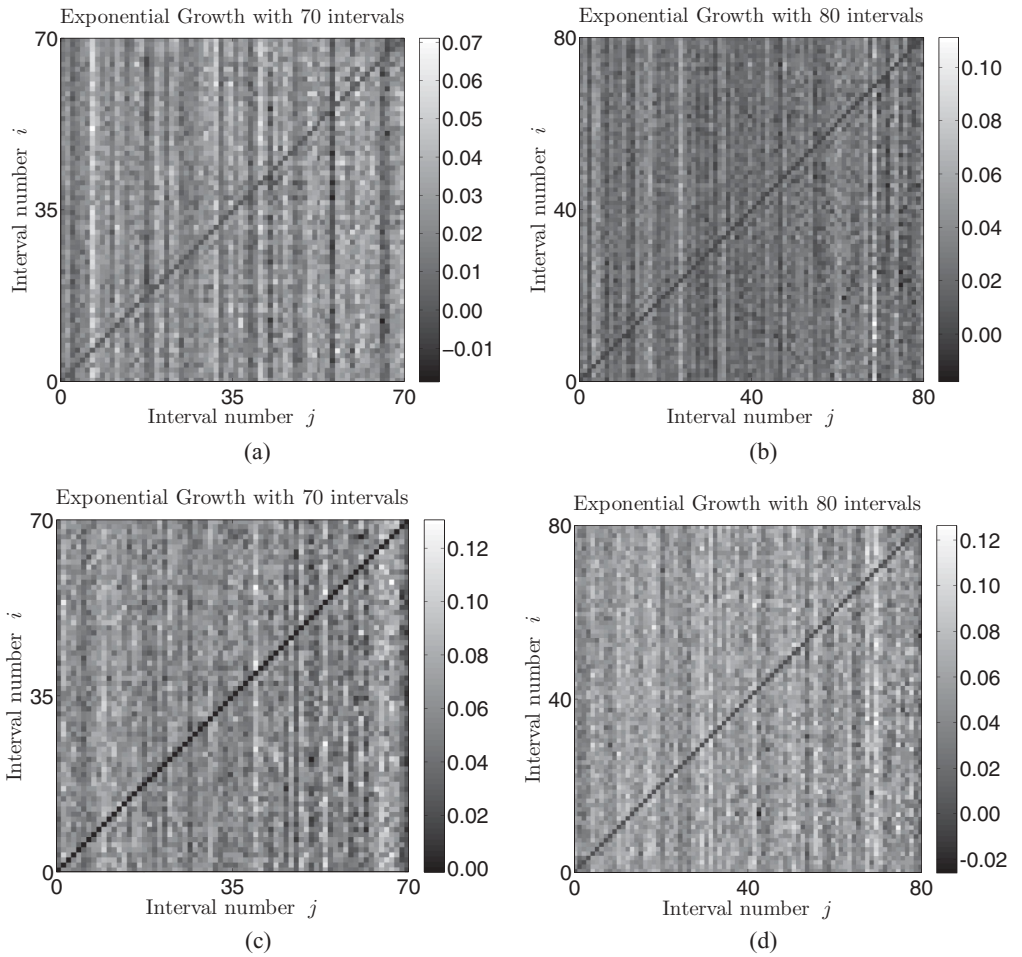

FIG. 12. Justification of the moment closure approximation. (a) and (b) show, for two different numbers of intervals, the relative error between the left-hand side and right-hand side of Eq. (65), given by Eq. (68), for an initially uniform domain that subsequently maintains a Voronoi partition. (c) and (d) show the same quantity for the same numbers of intervals, again with an initially uniform domain partition, but with an interval-centered domain partition being maintained throughout the simulations. In all of the figures a dark band can be seen along the diagonal (i.e., $i = j$). For these values of i and j the values of l_i and l_j are the same, as are the values of $\langle l_i \rangle$ and $\langle l_j \rangle$. This means that the value of the relative error between the left-hand side and right-hand side of Eq. (65) is zero.

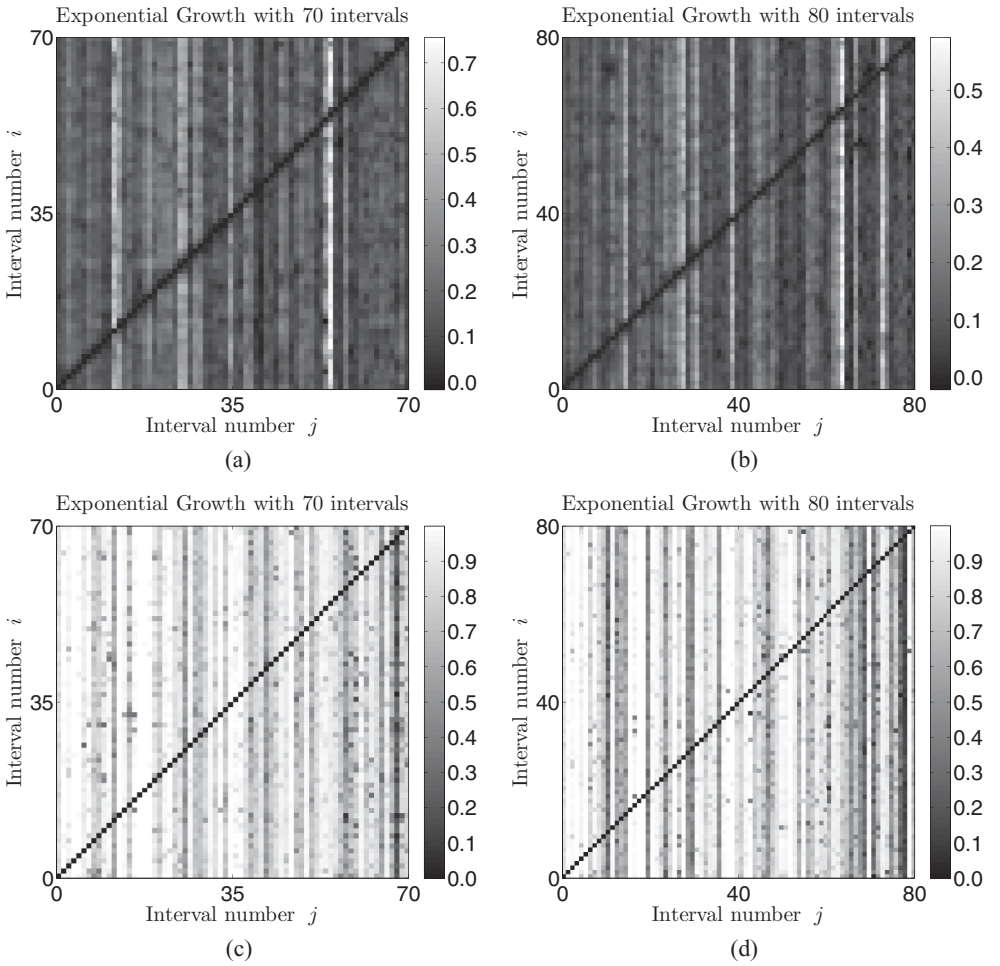

FIG. 13. Figures are as described in the caption of Fig. 12 with the exception that both simulations are initialized with an initially nonuniform domain partition.

for all values of i and j. Figure 12 shows the results of our investigations of the diffusion process for both the Voronoi and interval-centered domain partitions. In both simulations the domains are initially uniform and become nonuniform as a result of the stochastic growth of the domain. In both cases the moment closure approximation is extremely accurate throughout the field although, in general, the approximation is more accurate for the Voronoi partition [Figs. 12(a) and 12(b)] than for the interval-centered partition [Figs. 12(c) and 12(d)].

Figure 13 shows the results for diffusion with an initially nonuniform domain partition for both the Voronoi and interval-centered partitions. In both cases the moment closure approximation is less accurate than for the initially uniform domain. This is because an initially nonuniform domain is likely to give rise to small intervals. These intervals tend to grow less often than other intervals and as a consequence remain small throughout the simulation. Small intervals, in comparison to larger intervals, have larger fluctuations in particle density (as a consequence of the integer nature of particle numbers) and thus represent the mean-field particle density less well. In Figs. 13(a) and 13(b) the moment closure approximation is justified. In the case of the interval-centered partition small intervals have erroneously high particle numbers that distort the values for the average density and hence the moment closure approximations are generally slightly worse, but still good. There are large bands of intervals in Figs. 13(c) and 13(d) for which the moment closure approximation is poor. These results suggest that it is sensible to initialize the domain with a uniform or near-uniform partition so as to avoid small intervals and the associated decrease in accuracy that they harbor.

VII. CONCLUSION

A. Summary

We began this work, in Sec. II, by summarizing a stochastic position-jump framework for considering particle movement on a regular domain partition and demonstrated, via a continuous time RDME describing probability density, that the evolution of the mean density of particles in each interval can be linked to a PDE using a Taylor series expansion to convert from discrete space to continuous space. In Sec. III we generalized these results to a stochastic framework in which the domain partition was no longer uniform. In order to derive transition rates between nonuniform intervals we solved the first passage problem for an underlying microscopic process defined by a SDE and corresponding FPE. The derived transition rates were found to be a generalization of the

transition rates on the uniform domain partition. Numerical simulations were used to confirm the validity of our results.

Developing this equivalence framework between discrete microscale processes and continuum macroscale processes is important as it potentially allows us to base our models on experimental observations at an individual level and also to derive an equivalent description at the level of the whole population. These models provide us with a tool that is capable of representing both global and individual-level properties. Individual-level models are compatible with the incorporation of microscopic experimental data while the macroscopic PDE models allow us to extort the wide range of analytical tools available and to analyze the global properties of such models.

The main motivation for the consideration of nonuniform domain partitions was a more physically reasonable incorporation of domain growth into position-jump models than has previously been presented [14]. Instead of allowing intervals to instantaneously double in size and divide, in Sec. IV we made growth a more continuous process and loosened the coupling between interval growth and interval division, with intervals dividing only upon reaching a certain size. As a toy model we introduced deterministic domain growth in order to verify that domain growth could be implemented in an incremental fashion. However, we derived our main result pertaining to stochastic, incremental domain growth in Sec. V. We used a master equation formalism to show that the stochastic process of domain growth introduced in Sec. IV was equivalent to a classical PDE describing continuous exponential domain growth under some mild moment closure assumptions. We justified these assumptions, in Sec. VI, as well as corroborating our theoretical derivations with numerical simulations demonstrating the qualitative and quantitative equivalence of the stochastic and continuum models for diffusion.

B. Discussion

Position-jump models, such as the ones considered in this paper, are by no means the only individual-based models from which continuum models for particle density can be derived. Bodnar and Velazquez [22] and Murray *et al*. [23] derive continuum versions of off-lattice individual-based models in one dimension. Bellomo *et al*. [24] provide a useful overview of the use of asymptotic theory to transition from microscopic to macroscopic descriptions of particle migration, where the fundamental microscopic model employed is the velocity-jump process investigated in Refs. [8,12,13].

Considering on-lattice, individual-based models, it is often possible to write a probability master equation describing the evolution of the probability that a system is in a certain state. Turner *et al*. [9] use the probability master equation on a one-dimensional cellular Potts model incorporating interindividual adhesion in order to derive a linear diffusion equation whose diffusion coefficient can be linked explicitly to the model parameters. Alber *et al*. [10] extend this work into two dimensions.

The individual-level models that allow for the most straightforward derivation of a continuum limit are, like the models presented in this paper, on-lattice, position-jump models. Individuals are assumed to be points particles (as opposed to having finite size as in the cellular Potts model) and are restricted to (local) movement to one of their neighboring lattice sites with prescribed, possibly signal mediated, transition rates. Elementary examples of such discrete-continuum equivalence frameworks based on simple random walk models can be found in the influential texts of Berg [25] and Lin and Segel [26]. Codling *et al*. [27] also provide an overview of the derivation of continuum models of both biased and unbiased position-jump (or uncorrelated) random walks as well as their velocity-jump (or correlated) counterparts. Other authors who have dealt with on-lattice individual-based models via the RDME formalism approach adopted in this paper include Isaacson [28], Drawert *et al*. [29], and Ferm *et al*. [30].

The canonical model on which our work is founded is the position-jump (or "kangaroo," as they refer to it) model of Othmer *et al*. [8]. They are able to derive a continuum limit by considering an appropriate probability master equation and show, with a special choice of the jump kernel (so that only unbiased, discrete jumps of size Δ are allowed), that the continuum equation reduces to the diffusion equation.

At present we do not consider interactions between particles in our model. Painter and Hillen [2], however, do incorporate particle interaction into the transition rates of their on-lattice, individual-based model. Upon taking the continuum limit, in a similar manner to Othmer and Stevens [1], they arrive at a system of Keller-Segel-like equations.

The discrete-continuum equivalence frameworks on the stationary domain, built up in the above mentioned works, have inspired us to ask questions about how to appropriately incorporate domain growth into such frameworks. Domain growth has been successfully included in models of particle migration and such models have been used to demonstrate peak insertion and splitting in fish skin patterning [31,32]. Adapted chemotaxis models with volume filling have also been used to show that peak insertion or splitting is not a necessary result of pattern formation on a growing domain [2]. Using similar PDE models, Landman *et al*. [33] study a population of cells chemotaxing on a growing domain.

Despite these successes in a continuum setting, the realistic incorporation of domain growth into on-lattice, individual-level position-jump models has not previously been elucidated. In this paper we have built directly on our previous work [14] by attempting to make the method of domain growth in the individual model more physically reasonable. We combined a basic position-jump-type model with a domain growth method that allows the underlying lattice elements to grow incrementally. Using a further adapted master-equation-type formalism, we were able to derive a continuum equivalent to our model. Our numerical simulations demonstrate that this method of domain growth tends to make our individual-based models more similar to their continuum counterparts than our previous method. Despite the advances made in this current work there remains a multitude of related open problems.

C. Open problems

There are several possible avenues for further research. First, the domain partition dichotomy between the Voronoi and the interval-centered domain partitions is by no means perfect. It is obvious that on the stationary domain we should use the Voronoi partition to ensure the correct density of particles in

each interval. However, on the growing domain we cannot derive a closed-form PDE for cell density with the Voronoi partition due to the enforced nature of interval growth: Two intervals must grow at the same time in order to preserve the Voronoi property of the domain, thus preventing each interval from growing exponentially. We have demonstrated that the interval-centered domain partition allows us to derive a master equation that corresponds closely to the expected PDE for particle density on the growing domain. We have also seen, however, that the particle densities on this partition ultimately will not correspond to the mean-field densities. This poses a question as to whether some sort of domain partition duality might be more appropriate. The interval-centered domain partition may be employed to ensure the correct interval growth rates and the Voronoi domain partition used in order to find the correct particle densities (see Figs. S.5 and S.6 of Ref. [17]). Each time we require particle density it would be simple enough, keeping interval centers as fixed points, to find the corresponding Voronoi domain partition on which we might expect the particle density to be correct. This does, however, pose questions as to what exactly we mean by particle density. Even more troubling, from a computational point of view, is the situation in which particle migration or domain growth are dependent on density. This would require conversion from the interval-centered to the Voronoi domain partition at every time step, which would surely lead to a large increase in simulation times.

Second, the question of robust pattern formation for stochastic processes on growing domains is one of much biological and mathematical interest [34,35]. Until now there has been no method to simulate such stochastic processes robustly, without artificially changing the nature of the pattern formed by implementing instantaneous growth and division events. We envisage that our incremental interval growth method, and its corresponding PDE, will be of great interest to mathematicians and biologists alike, allowing for the correct simulation of stochastic pattern formation and evolution even with strong ubiquitous growth.

Third, the two-way coupling between particle migration and tissue growth is important from a biological point of view. Not only does growth affect the movement of the particles on the domain, but the particles can also feed back and affect growth of the domain [15,36]. In our previous work [14] we were able to incorporate different mechanisms of domain growth (including density-dependent growth) into our discrete-continuum equivalence framework. This has yet to be accomplished for our more physically reasonable method of domain growth but, given the insights gained in this paper with regard to the necessity of the Voronoi domain partition for the calculation of the correct particle densities, we have provided the platform to make this possible.

Finally, we have yet to apply the domain growth modeling work presented in this paper to experimental systems. There are many possibilities that we might consider. Kruse [16] presents an initially individual-based one-dimensional position-jump model for the localization of the division septum in dividing *Escherichia coli* bacterial cells. As an approximation, the time scale of the localization is assumed to be fast in comparison to the time scale of growth and hence the effects of growth are neglected. Our modeling regime would potentially allow for the effects of domain growth on the localization of the division septum to be explored in the context of Kruse's model.

The goal of our research is to provide insights into the mechanisms underlying the movement of individuals (be they inert particles, proteins, or cells) on growing domains. The work of Kruse [16] is just one of many potential applications of the modeling regime we have presented in this paper. It seems prudent that, in applying our modeling paradigm to biological situations, further model analysis and parametrization, followed by repeats of the alter-predict-test cycle, should be carried out in order to suggest ways in which the models should be improved.

ACKNOWLEDGMENTS

C.A.Y. would like to thank Christ Church, Oxford for support through a Junior Research Fellowship. P.K.M. was partially supported by a Royal Society Wolfson Research Merit Award.

[1] H. G. Othmer and A. Stevens, SIAM J. Appl. Math. **57**, 1044 (1997).
[2] K. J. Painter and T. Hillen, Can. Appl. Math. Quart. **10**, 501 (2002).
[3] M. J. Simpson, K. A. Landman, and B. D. Hughes, Physica A **388**, 399 (2009).
[4] R. Erban, I. G. Kevrekidis, D. Adalsteinsson, and T. C. Elston, J. Chem. Phys. **124**, 084106 (2006).
[5] I. G. Kevrekidis, C. W. Gear, J. M. Hyman, P. G. Kevrekidis, O. Runborg, and C. Theodoropoulos, Comm. Math. Sci. **1**, 715 (2003).
[6] C. A. Yates, R. Erban, C. Escudero, I. D. Couzin, J. Buhl, I. G. Kevrekidis, P. K. Maini, and D. J. T. Sumpter, Proc. Natl. Acad. Sci. USA **106**, 5464 (2009).
[7] C. Escudero, C. A. Yates, J. Buhl, I. D. Couzin, R. Erban, I. G. Kevrekidis, and P. K. Maini, Phys. Rev. E **82**, 011926 (2010).
[8] H. G. Othmer, S. R. Dunbar, and W. Alt, J. Math. Biol. **26**, 263 (1988).
[9] S. Turner, J. A. Sherratt, K. J. Painter, and N. J. Savill, Phys. Rev. E **69**, 021910 (2004).
[10] M. Alber, N. Chen, P. M. Lushnikov, and S. A. Newman, Phys. Rev. Lett. **99**, 168102 (2007).
[11] T. Hillen and K. J. Painter, J. Math. Biol. **58**, 183 (2009).
[12] T. Hillen and H. G. Othmer, SIAM J. Appl. Math. **61**, 751 (2000).
[13] H. G. Othmer and T. Hillen, SIAM J. Appl. Math. **62**, 1222 (2002).
[14] R. E. Baker, C. A. Yates, and R. Erban, Bull. Math. Biol. **72**, 719 (2010).

[15] A. M. Smith, R. E. Baker, D. Kay, and P. K. Maini, J. Math. Biol. (2011), doi:10.1007/s00285-011-0464-y.
[16] K. Kruse, Biophys. J. **82**, 618 (2002).
[17] See Supplemental Material at http://link.aps.org/supplemental/10.1103/PhysRevE.86.021921 for more details and movies.
[18] S. Redner, *A Guide to First-Passage Processes* (Cambridge University Press, Cambridge, 2001).
[19] S. Engblom, L. Ferm, A. Hellander, and P. Lötstedt, SIAM J. Sci. Comput. **31**, 1774 (2009).
[20] D. T. Gillespie, J. Phys. Chem. **81**, 2340 (1977).
[21] F. Spitzer, Adv. Math. **5**, 246 (1970).
[22] M. Bodnar and J. J. L. Velazquez, Math. Methods Appl. Sci. **28**, 1757 (2005).
[23] P. J. Murray, C. M. Edwards, M. J. Tindall, and P. K. Maini, Phys. Rev. E **80**, 031912 (2009).
[24] N. Bellomo, A. Bellouquid, J. Nieto, J. Soler, and F. Brezzi, Math. Models Methods Appl. Sci. **22**, 1130001 (2012).
[25] H. C. Berg, *Random Walks in Biology* (Princeton University Press, Princeton, 1993).
[26] C. C. Lin and L. A. Segel, *Mathematics Applied to Deterministic Problems in the Natural Sciences*, Vol. 1. (Macmillan, New York, 1988).
[27] E. A. Codling, M. J. Plank, and S. Benhamou, J. R. Soc. Int. **5**, 813 (2008).
[28] S. A. Isaacson, SIAM J. Appl. Math. **70**, 77 (2009).
[29] B. Drawert, M. J. Lawson, L. Petzold, and M. Khammash, J. Chem. Phys. **132**, 074101 (2010).
[30] L. Ferm, A. Hellander, and P. Lötstedt, J. Comput. Phys. **229**, 343 (2010).
[31] K. J. Painter, P. K. Maini, and H. G. Othmer, Proc. Natl. Acad. Sci. USA **96**, 5549 (1999).
[32] S. Kondo and R. Asai, Nature **376**, 765 (2002).
[33] K. A. Landman, G. J. Pettet, and D. F. Newgreen, Bull. Math. Biol. **65**, 235 (2003).
[34] B. J. Binder and K. A. Landman, J. Theor. Biol. **259**, 541 (2009).
[35] T. E. Woolley, R. E. Baker, E. A. Gaffney, and P. K. Maini, Phys. Rev. E **84**, 021915 (2011).
[36] L. Hufnagel, A. A. Teleman, H. Rouault, S. M. Cohen, and B. I. Shraiman, Proc. Natl. Acad. Sci. USA **104**, 3835 (2007).